A dynamic H3K27ac signature identifies VEGFA-stimulated endothelial enhancers and requires EP300 activity

Bing Zhang, Daniel S. Day, Joshua W. Ho, et al.

Genome Res. 2013 23: 917-927 originally published online April 1, 2013
Access the most recent version at doi:10.1101/gr.149674.112

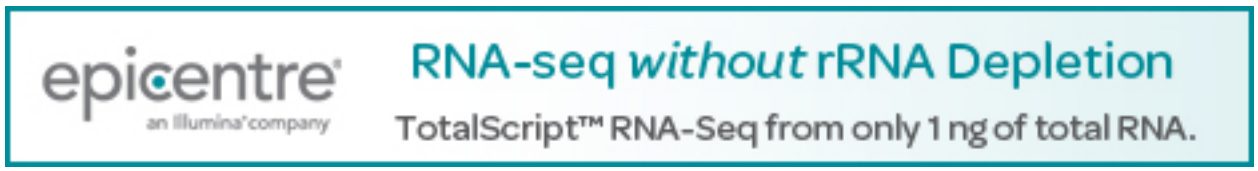

A dynamic H3K27ac signature identifies VEGFA-stimulated endothelial enhancers and requires EP300 activity

Bing Zhang,[1,7] Daniel S. Day,[2,3,7] Joshua W. Ho,[2] Lingyun Song,[4] Jingjing Cao,[1] Danos Christodoulou,[5] Jonathan G. Seidman,[5] Gregory E. Crawford,[4] Peter J. Park,[2] and William T. Pu[1,6,8]

[1]*Department of Cardiology, Boston Children's Hospital, Boston, Massachusetts 02115, USA;* [2]*Center for Biomedical Informatics, Harvard Medical School, Boston, Massachusetts 02115, USA;* [3]*Harvard/MIT Division of Health Sciences and Technology, Cambridge, Massachusetts 02139, USA;* [4]*Institute for Genome Sciences & Policy, Duke University, Durham, North Carolina 27708, USA;* [5]*Department of Genetics, Harvard Medical School, Boston, Massachusetts 02114, USA;* [6]*Harvard Stem Cell Institute, Harvard University, Cambridge, Massachusetts 02138, USA*

Histone modifications are now well-established mediators of transcriptional programs that distinguish cell states. However, the kinetics of histone modification and their role in mediating rapid, signal-responsive gene expression changes has been little studied on a genome-wide scale. Vascular endothelial growth factor A (VEGFA), a major regulator of angiogenesis, triggers changes in transcriptional activity of human umbilical vein endothelial cells (HUVECs). Here, we used chromatin immunoprecipitation followed by high-throughput sequencing (ChIP-seq) to measure genome-wide changes in histone H3 acetylation at lysine 27 (H3K27ac), a marker of active enhancers, in unstimulated HUVECs and HUVECs stimulated with VEGFA for 1, 4, and 12 h. We show that sites with the greatest H3K27ac change upon stimulation were associated tightly with EP300, a histone acetyltransferase. Using the variation of H3K27ac as a novel epigenetic signature, we identified transcriptional regulatory elements that are functionally linked to angiogenesis, participate in rapid VEGFA-stimulated changes in chromatin conformation, and mediate VEGFA-induced transcriptional responses. Dynamic H3K27ac deposition and associated changes in chromatin conformation required EP300 activity instead of altered nucleosome occupancy or changes in DNase I hypersensitivity. EP300 activity was also required for a subset of dynamic H3K27ac sites to loop into proximity of promoters. Our study identified thousands of endothelial, VEGFA-responsive enhancers, demonstrating that an epigenetic signature based on the variation of a chromatin feature is a productive approach to define signal-responsive genomic elements. Further, our study implicates global epigenetic modifications in rapid, signal-responsive transcriptional regulation.

[Supplemental material is available for this article.]

Genome-wide profiling of chromatin components between different cell types has demonstrated that transcriptional regulatory elements are decorated by characteristic patterns of post-translational histone modifications and other chromatin features and that these features contribute to cell type-specific gene regulation (Heintzman et al. 2007; Ernst et al. 2011; Kharchenko et al. 2011; Bonn et al. 2012). Such epigenetic signatures have been used to functionally annotate transcriptional regulatory elements that distinguish different cell types. For example, active enhancers, genomic elements that stimulate gene transcription, are marked by acetylation of histone H3 at lysine 27 (H3K27ac) (Creyghton et al. 2010; Kharchenko et al. 2011; Rada-Iglesias et al. 2011; Zentner et al. 2011), the presence of the chromatin regulator EP300 (Visel et al. 2009; Creyghton et al. 2010), hypersensitivity to nuclease digestion (Boyle et al. 2008), and expression of RNA transcripts known as eRNAs (Kim et al. 2010; Wang et al. 2011). However, much less is known about how chromatin signatures change during rapid cellular responses to extracellular cues and the effectiveness of epigenetic profiles in identifying transcriptional elements that mediate signal-responsive changes in gene expression.

We studied rapid, signal-responsive changes in chromatin features using vascular endothelial growth factor A (VEGFA)-stimulated endothelial cells as a model system. Blood vessels nourish nearly every organ. Their growth is tightly regulated, and inadequate, excessive, or abnormal blood vessel growth is linked to a panoply of diseases, including ischemic heart disease, blinding eye diseases, and cancer (Carmeliet and Jain 2011). A central regulator of blood vessel growth is vascular endothelial growth factor A. In response to VEGFA signaling, endothelial cells dramatically change their phenotype and gene expression profile (Schweighofer et al. 2009). Intracellular signaling downstream from VEGFA has been studied in depth, but relatively less is known about the transcriptional regulatory elements that respond to VEGFA signaling.

We profiled activating chromatin epigenetic marks in a 12-h time course of endothelial cell stimulation by VEGFA. We show that temporal variation of H3K27ac is a novel epigenetic signature that identifies VEGFA-regulated enhancers and predicts VEGFA-responsive gene expression. Our work further shows that the

[7]**These authors contributed equally to this work.**
[8]**Corresponding author**
E-mail wpu@pulab.org
Article published online before print. Article, supplemental material, and publication date are at http://www.genome.org/cgi/doi/10.1101/gr.149674.112.

catalytic activity of EP300 is required for dynamic changes in H3K27ac occupancy, altered chromatin architecture, and regulation of gene expression by VEGFA.

Results

VEGFA-induced changes in H3K27ac

To study transcriptional and epigenetic regulation during angiogenesis, we measured H3K27ac chromatin occupancy genome-wide in human umbilical vein endothelial cells (HUVECs) treated for 0 (unstimulated), 1, 4, and 12 h with VEGFA (Supplemental Table 1). Overall, our ChIP-seq data correlated with H3K27ac in ENCODE data sets, with some differences likely attributable to differences in growth conditions (Supplemental Fig. 1). Inspection of the H3K27ac ChIP-seq data showed regions with substantial changes in H3K27ac as a result of VEGFA stimulation (boxed regions, Fig. 1A,B). To identify regions with VEGFA-induced variation in H3K27ac, we calculated the H3K27ac signal-normalized variance (variance score) for 200-bp sliding windows across the 12-h time course. This approach captured thousands of regions with substantial VEGFA-induced variation (Fig. 1C). Out of sites with a $\log_2$ variance score greater than 3, we selected those near eight genes implicated in angiogenesis for validation by ChIP-qPCR. Sites near six genes were successfully assayed, and, in all six cases, the ChIP-qPCR results were consistent with the ChIP-seq data (Fig. 1D).

A dynamic VEGFA-regulated H3K27ac signature is tightly linked to EP300 chromatin occupancy

The transcriptional coactivator EP300 acetylates histones (Ogryzko et al. 1996) and occupies tissue-specific enhancers (Visel et al. 2009). To define the relationship of EP300 chromatin occupancy to dynamic H3K27ac sites, we measured EP300 chromatin occupancy during the VEGFA stimulation time course by ChIP-seq. The EP300 ChIP-seq data were reproducible between independent biological duplicates (Pearson r > 0.92) (Supplemental Fig. 2A). Comparison to publicly available ENCODE EP300 occupancy data for the immortalized B-cell cell line GM12878 (Reddy et al. 2012) indicated that EP300 binding was largely cell type-specific (Supplemental Fig. 2B). Next, from the VEGFA time course data, we calculated the distance from EP300 sites to neighboring H3K27ac

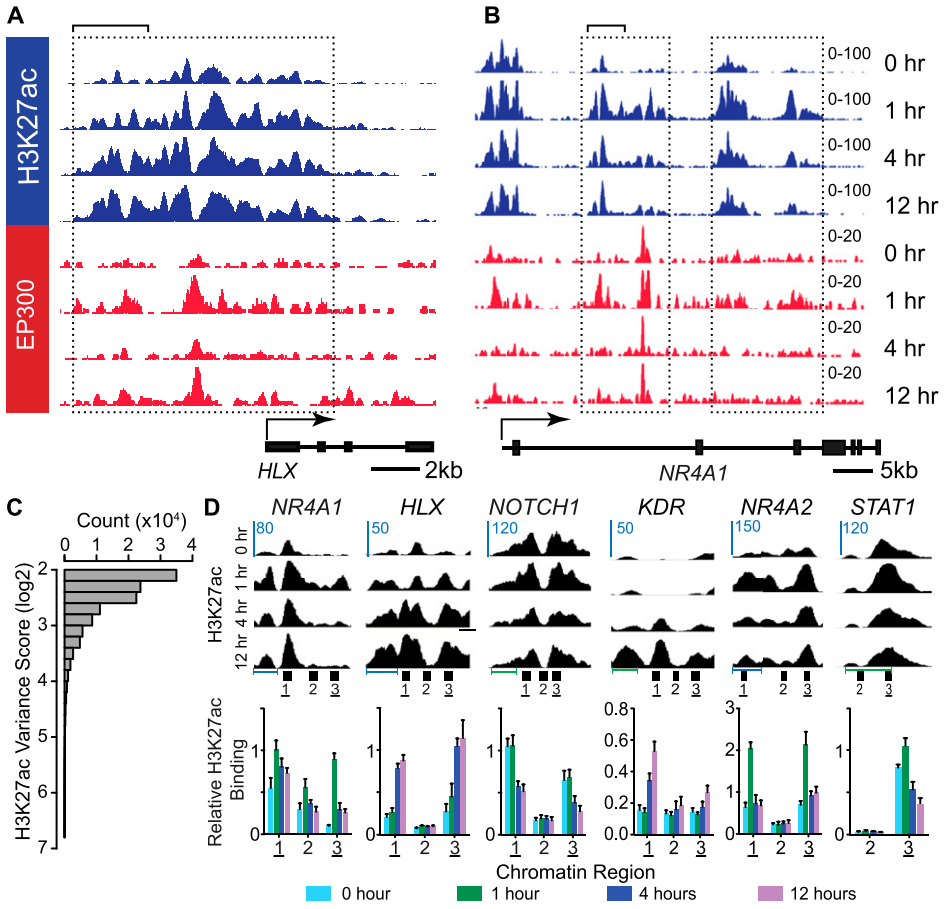

Figure 1. VEGFA-stimulated dynamic changes in H3K27ac occupancy. (*A*,*B*) Browser views of H3K27ac and EP300 ChIP-seq enrichment at *HLX* and *NR4A1* at four time points following VEGFA stimulation. Note areas with varying H3K27ac occupancy in response to VEGFA (boxed regions). Bracketed regions are enlarged in portions of panel *C*. (*C*) H3K27ac variance score histogram. VEGFA-stimulated significant changes in H3K27ac regions during the 12-h time course. The plot only includes regions with a $\log_2$ variance score greater than or equal to 2. (*D*) Chip-qPCR validation of VEGFA-induced changes in H3K27ac occupancy. Browser views show ChIP-seq enrichment, and lower plots indicate H3K27ac ChIP-qPCR using numbered amplicons indicated in the browser views. Underlined numbers indicate regions where ChIP-seq predicted VEGFA-stimulated H3K27ac occupancy change, while regions without underline are adjacent controls. Horizontal scale bars: (blue) 1 kb, (green) 0.5 kb.

sites, stratified by their H3K27ac variance score. Interestingly, most of the regions with the greatest H3K27ac variance scores occurred within 2 kb of EP300 sites, while less variant H3K27ac sites tended to be further from EP300 (Fig. 2A; Supplemental Fig. 3). This result supported a tight relationship between EP300 and dynamic but not static H3K27ac marks.

The enrichment of EP300 near dynamic H3K27ac sites suggested that EP300 is functionally involved in deposition of H3K27ac in response to VEGFA stimulation. To test the functional requirement for EP300 in VEGFA-stimulated deposition of H3K27ac, we measured the effect of EP300 knockdown on H3K27ac chromatin occupancy. siRNA EP300 knockdown (Supplemental Fig. 4) blocked VEGFA-stimulated deposition of H3K27ac at *NR4A1*, *HLX*, and *KDR* (Fig. 2B; Supplemental Fig. 5A). To determine if EP300 histone acetyltransferase catalytic activity, as opposed to other functions mediated by EP300 (e.g., coactivator complex formation through protein-protein interactions), is required for VEGFA-stimulated H3K27ac, we inhibited EP300 enzymatic activity using the small molecule C646 (Bowers et al. 2010). Pretreatment of HUVEC cells for 30 min with C646 blocked VEGFA-stimulated deposition of H3K27ac (Fig. 2C; Supplemental Fig. 5B).

We next interrogated the extent to which EP300 activity is required for dynamic H3K27ac deposition genome-wide by performing H3K27ac ChIP-seq on cells pretreated with C646 and then stimulated with VEGFA for 0, 1, and 4 h. The cells became unhealthy by 12 h, precluding analysis at this time point. This experiment demonstrated that EP300 inhibition caused widespread reduction in H3K27ac variation induced by VEGFA (Fig. 2D; Supplemental Fig. 5C,D). However, some VEGFA-stimulated changes in H3K27ac persisted, indicating that additional mechanisms also contribute to H3K27ac changes induced by VEGFA. Overall, these data indicate a key role of EP300 in contributing to H3K27 acetylation induced by VEGFA.

Changes in nucleosome positioning were previously reported to underlie rapid changes in the occupancy profile of histone H3 dimethylated at lysine 4 (H3K4me2) (He et al. 2010). We tested the hypothesis that changes in nucleosome occupancy contribute to the observed dynamic changes in H3K27ac by measuring total histone H3 and H3K4me2 occupancy at six dynamic H3K27ac sites (Fig. 2E; Supplemental Fig. 6). We did not observe significant changes in histone H3 or H3K4me2 occupancy at any of these sites, indicating that acetylation of histone H3 rather than shifts in its position cause altered H3K27ac occupancy.

Temporal clustering of H3K27ac variation defined groups of chromatin regions with distinct function annotations and enriched transcription factor motifs

To investigate the significance of EP300-associated variation in H3K27ac, we focused on the subset of H3K27ac sites within 2 kb of EP300 with the highest variance scores (upper 20th percentile) (see Methods; Supplemental Table 2; Supplemental Fig. 3). Hierarchical clustering showed that H3K27ac enrichment at these sites followed three predominant temporal patterns (Fig. 3A). We labeled these clusters as H1 (peak H3K27ac signal at 1 h; 4689 regions), H4-12 (peak H3K27ac signal at 4–12 h; 3947 regions), and H0 (decreased H3K27ac signal at 4–12 h; 3601 regions). Plotting H3K27ac signal intensity for each region illustrated the significant dynamic changes of H3K27ac binding in each temporal cluster (Fig. 3B; Supplemental Fig. 7A). Cluster H4-12 was particularly interesting, because it showed initial depletion of H3K27ac signal at the peak center at 0 and 1 h and subsequent "filling-in" of the depleted region at 4 and 12 h (Fig. 3B; Supplemental Fig. 7A).

Our genome-wide analysis of the effect of the EP300 inhibitor C646 on VEGFA-stimulated H3K27 acetylation showed a mechanistic requirement for EP300 at the majority of sites. We, therefore, examined the C646 effect on the H1, H4-12, and H0 clusters in detail. Consistent with its essential role in VEGFA-stimulated deposition of H3K27ac, C646 strongly blunted H3K27ac accumulation in the H1 and H4-12 clusters (Fig. 3C; Supplemental Fig. 7B). Interestingly, the down-regulation of H3K27ac seen in the H0 cluster was also blunted by C646, suggesting secondary effects on counter-regulatory mechanisms that remove H3K27ac marks.

When the regions were centered on EP300 enrichment, aggregation plots of H3K27ac signal showed that maximal H3K27ac signal variation occurred adjacent to, rather than overlapping, EP300 (Fig. 3D). Prior work showed that the chromatin landscape at most transcription factor binding sites is asymmetric. When we applied an algorithm for function strand segregation (Kundaje et al. 2012), we found that H3K27ac and EP300 occupancy were both asymmetric in the H1, H4-12, and H0 clusters (Supplemental Fig. 7C). Interestingly, the distribution of H3K27ac and EP300 with respect to the peak center was largely concordant, consistent with a mechanistic role of EP300 in establishing the H3K27ac marks.

EP300 aggregation plots showed that EP300 binding also changed during the VEGFA-stimulation time course (Fig. 3E). We confirmed VEGFA-stimulated enrichment of EP300 by ChIP-qPCR (Supplemental Fig. 7D). For cluster H4-12, on average, EP300 binding increased before H3K27ac occupancy. At cluster H1, these events appear to occur concurrently, suggesting that either the sequence of events differs at 1 h or that the data did not contain sufficient temporal resolution to order events peaking at this early time point. For cluster H0 with decreasing H3K27ac signal, EP300 signal increased at 1 h, but H3K27ac signal did not (Fig. 3B–E; Supplemental Fig. 7D), suggesting that other factors, such as increased HDAC activity, impeded H3K27ac deposition at these regions.

We further characterized the location and function of the dynamic, EP300-associated H3K27ac sites. Most of these sites were located distal to transcriptional start sites (TSSs) of genes, consistent with the reported predominant location of EP300 (Visel et al. 2009; Creyghton et al. 2010). However, a significantly greater proportion of sites in cluster H1 were located in promoters, near gene TSSs (P-value < 10^{-46}), while a significantly greater proportion of sites in cluster H4-12 were located in intergenic regions (P-value < 10^{-10}) (Fig. 4A). Dynamic, EP300-associated H3K27ac sites were associated with 8454 adjacent genes. The majority of these genes did not overlap between temporal H3K27ac clusters (Fig. 4B). Gene Ontology (GO) analysis showed that these different gene sets have distinct functional properties (Fig. 4C). Both of the late-responding clusters, H4-12 and H0, were strongly enriched for terms related to vascular development, endothelial differentiation, and angiogenesis. In contrast, the early-responding H1 cluster was enriched for terms related to cell morphology, protein metabolism, response to oxygen levels, and TGFbeta receptor signaling, which are relevant to cellular stress responses in many cells types, including endothelial cells. Collectively, our data indicate that each temporal cluster of dynamic EP300-associated H3K27ac sites was linked to regulation of varying aspects of cellular function.

To identify transcription factors that regulate EP300 recruitment and VEGFA-regulated H3K27 acetylation, we searched for overrepresented transcription factor binding motifs among sequences at EP300 peaks in each cluster. De novo motif discovery revealed highly significant enrichment of ETS, FOX, AP1, STAT, and SP1 families in all three clusters. To further validate the motif discovery results, we performed ChIP-seq for ETS1 and found that 51% of EP300-bound regions were co-occupied by ETS1 (Fig. 4E).

Our analysis also identified transcription factor motifs that occurred in one or two of the H3K27ac clusters. The motif of ATF and CREB1, mediators of immediate early responses in multiple cell types (Altarejos and Montminy 2011), was significantly enriched in the H1 cluster. Also notable was overrepresentation of the SMAD binding motif in the H1 cluster, where we observed enrichment for the TGFbeta receptor signaling pathway (Fig. 4D). We found overrepresentation of GATA and TEAD binding motifs (Fig. 4D; Supplemental Table 3) in the H0 and H4-12 clusters, while the binding motif of RBP/J, the nuclear target of Notch signaling, was enriched in the H0 and H1 clusters (Fig. 4D; Supplemental Table 3). These results suggest that members of these transcription factor families are important in orchestrating EP300 recruitment and H3K27ac deposition in response to VEGFA stimulation.

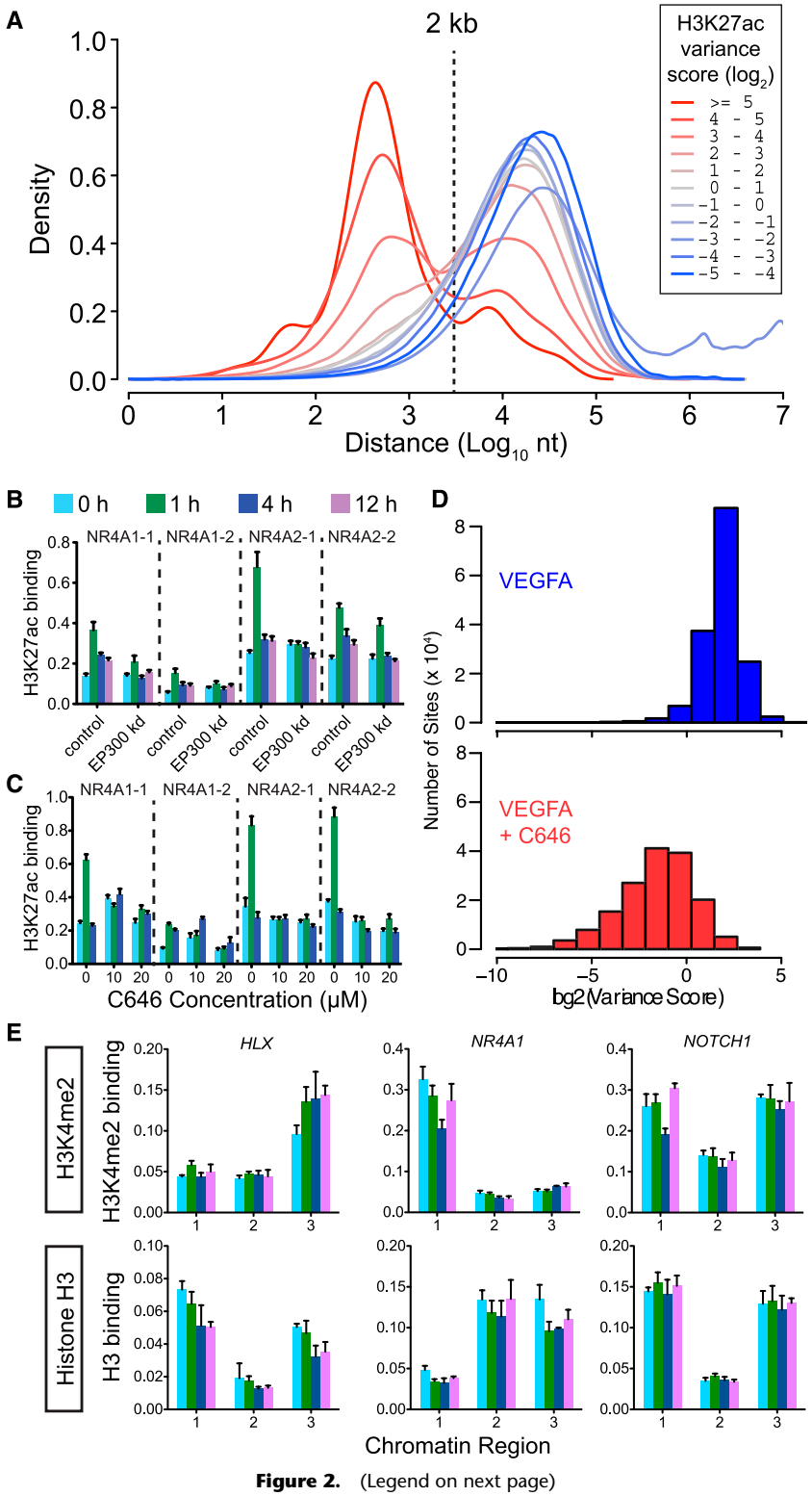

Figure 2. (Legend on next page)

Enrichment of TF motifs at dynamic H3K27ac sites suggested that these TFs recruit EP300 and thereby contribute to changes in H3K27ac. To test this hypothesis, we knocked down ETS1 or C-JUN (a component of the AP1 heterodimer) and measured the effect on dynamic H3K27ac sites directly bound by these factors. Validation experiments demonstrated efficient ETS1 or C-JUN knockdown in HUVECs after siRNA transfection (Supplemental Fig. 8A,B,E,F) and corresponding reduction of ETS1 or JUN (also known as c-Jun) occupancy of tested dynamic H3K27ac sites (two sites tested per factor) (Supplemental Fig. 8C,G). This reduction of ETS1 or JUN binding attenuated H3K27ac changes at these sites in response to VEGFA (Supplemental Fig. 8D,H). These results suggest that TFs with enriched motifs are functionally important in mediating dynamic H3K27ac changes in response to VEGFA.

The dynamic H3K27ac signature defines VEGFA-responsive transcriptional regulatory elements

Active transcriptional regulatory elements are characterized by hypersensitivity to digestion by DNase I (Xi et al. 2007). To further investigate whether dynamic, EP300-associated H3K27ac sites are activating transcriptional regulatory elements, we performed genome-wide measurement of DNase I hypersensitivity during the VEGFA-stimulation time course using DNase-seq (Boyle et al. 2008). Biological duplicate samples showed that the technique is highly reproducible (Supplemental Fig. 9A). Dynamic, EP300-associated H3K27ac loci were DNase I hypersensitive (Fig. 5A), consistent with their function as active transcriptional regulatory elements. Interestingly, on average, these regions did not change significantly in their sensitivity to DNase I digestion during the VEGFA-stimulation time course (Fig. 5A; Supplemental Fig. 9B–D), suggesting that most of these

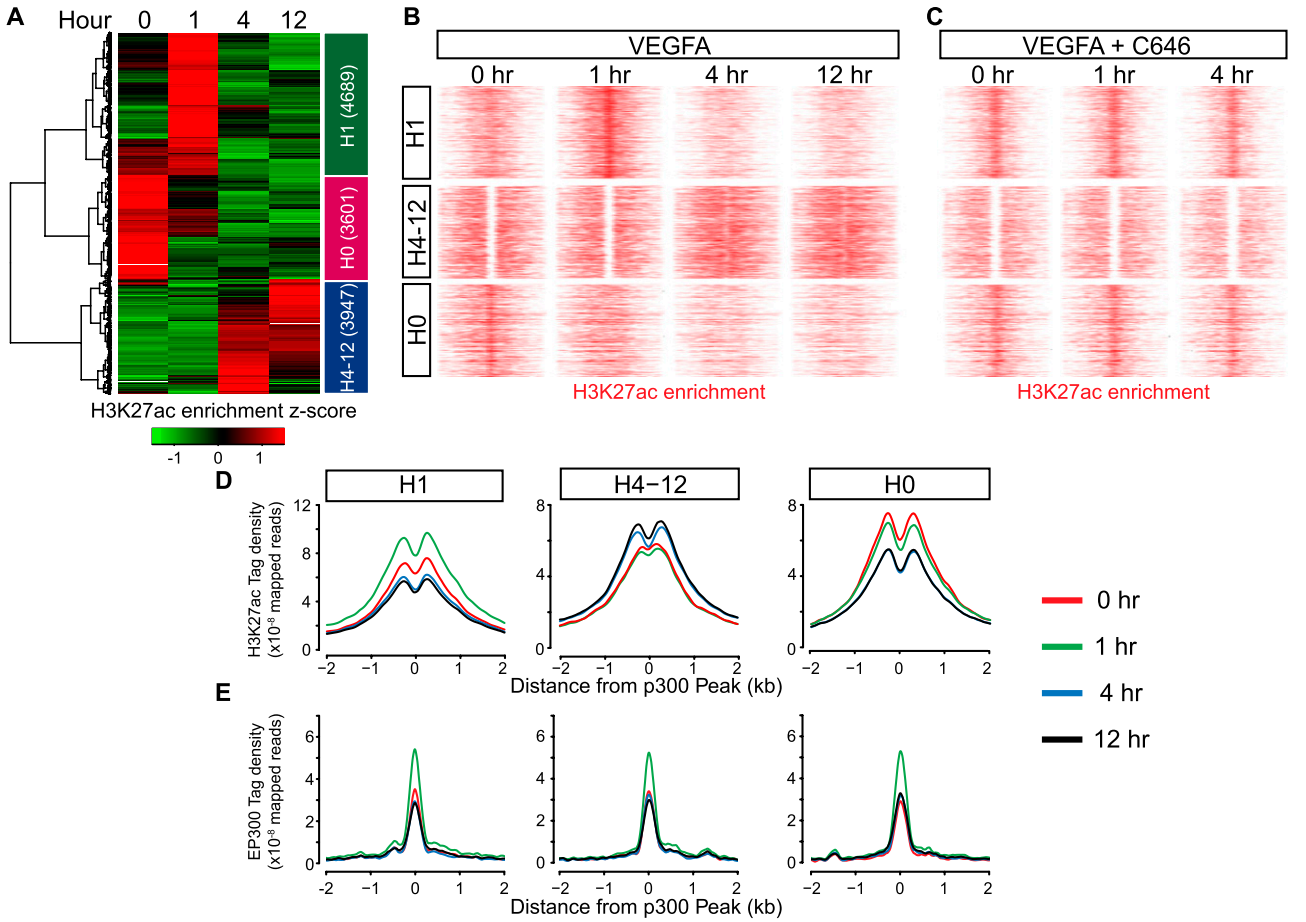

Figure 3. Dynamic, EP300-associated H3K27ac regions grouped into three temporal clusters. (*A*) Hierarchical clustering heat map of dynamic EP300-associated H3K27ac variants. Cluster names and number of regions per cluster are indicated in the adjacent colored bar. (*B*,*C*) Tag density map of dynamic H3K27ac clusters during VEGFA stimulation time course, without (*B*) or with (*C*) the EP300 inhibitor C646. Each row represents a 4-kb region centered on a dynamic H3K27ac site. The same color scale was applied within each cluster. Note the loss of VEGFA-induced changes of H3K27 acetylation. (*D*) H3K27ac aggregation plots, centered on nearby EP300 peaks. Maximal H3K27ac density occurred adjacent to EP300 peak centers. (*E*) EP300 aggregation plots, centered on EP300 peaks within 2 kb of dynamic H3K27ac regions.

sites are already "open" and poised to respond to VEGFA stimulation. These data are consistent with our observation that H3K27 acetylation was not associated with changes in nucleosome occupancy (Fig. 2D; Supplemental Fig. 6).

Active enhancers are also characterized by production of transcripts known as eRNAs (Kim et al. 2010). To further characterize the dynamic, EP300-associated H3K27ac loci and confirm their enhancer activity, we measured eRNA transcript levels from the activating clusters (H1 and H4-12) by qRT-PCR (Fig. 5B; Supplemental Fig. 10A), testing 11 regions distal to gene bodies. In regions belonging to cluster H1, eRNA was strongly up-regulated at 1 h and then decreased at 4 and 12 h. In regions belonging to cluster H4-12, eRNA was up-regulated to maximal levels by 1 h and was sustained through hours 4 and 12. As controls, we measured eRNA transcripts from nearby regions with H3K27ac enrichment that did not change during the VEGFA time course. Although some control regions also showed VEGFA-stimulated changes in transcript level, their number and overall fold increase were less than at H3K27ac dynamic regions (Supplemental Fig. 10A).

H4-12 cluster regions showed increased EP300 recruitment and eRNA activity at 1 h, whereas H3K27ac did not increase until 4–12 h. To determine if EP300 activity was required for VEGFA-stimulated increases in eRNA, we blocked EP300 activity with C646 and measured eRNA levels. We found that acute EP300

Figure 2. Dynamic H3K27ac regions were associated with EP300. (*A*) Distance relationship of H3K27ac sites to nearest EP300-occupied region as a function of H3K27ac variance score. The H3K27ac regions with the highest variance score were predominantly located within 2 kb of EP300. (*B*,*C*) EP300 is required for dynamic H3K27 acetylation. ChIP-qPCR of H3K27ac in HUVEC cells treated with VEGFA and EP300 siRNA (*B*) or small molecule EP300 acetyltransferase inhibitor C646 (*C*). Two dynamic H3K27ac regions near each of the indicated four genes were tested (see also Supplemental Fig. 5A,B). (*D*) C646 pretreatment suppresses H3K27ac change at highly variant sites. We considered genomic windows with a $\log_2$ variance score of at least 2 and at least the sum of 10 reads across all four time points. We recalculated the variance score for each site under VEGFA stimulation in the absence or presence of C646 for hours 0, 1, and 4. The histogram shows that C646 reduced the variance score at the vast majority of sites. (*E*) Chip-qPCR of H3K4me2 and total histone H3 binding at three dynamic H3K27ac sites showed that altered nucleosome positioning is unlikely to account for VEGFA-stimulated changes in H3K27ac. Numbered chromatin regions are indicated in Fig. 1D.

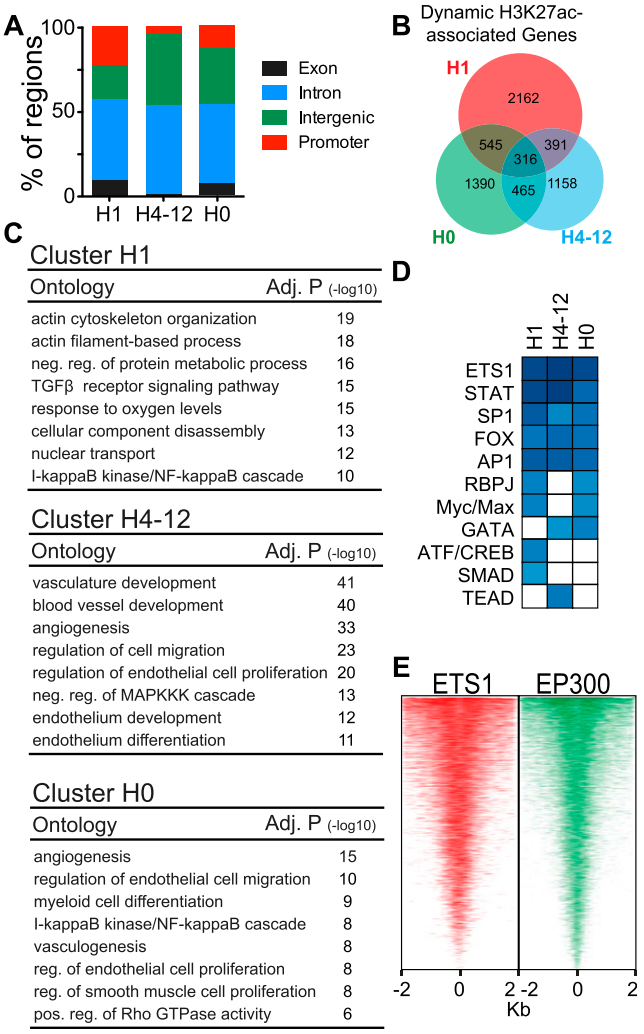

Figure 4. Characterization of dynamic, EP300-associated H3K27ac regions. (*A*) Genomic distribution of dynamic H3K27ac regions. (*B*) Venn diagram of genes associated with the three clusters of dynamic H3K27ac regions. (*C*) Biological process terms were selected from the 20 most significantly enriched for dynamic H3K27ac regions. (*D*) Transcription factor families with enriched motifs found under EP300 peaks at dynamic H3K27ac regions. Color intensity indicates significance score (see Supplemental Table 3 for full table). (*E*) ETS1 and EP300 colocalized near dynamic H3K27ac regions. ETS1 and EP300 tag densities are plotted in EP300-bound regions, sorted by ETS1 tag enrichment.

inhibition blocked VEGFA-stimulated up-regulation of eRNA (Fig. 5B; Supplemental Fig. 10B). In the H1 cluster, our experiments were unable to resolve temporal differences in EP300 recruitment, eRNA activity, and H3K27ac binding, which concurrently peaked at 1 h. Nevertheless, EP300 inhibition also blocked eRNA up-regulation at H1 regions, suggesting a similar role of EP300 in this cluster. Our results suggest that EP300 recruitment and acetylase activity are required for eRNA synthesis and precedes H3K27 acetylation.

Since the dynamic EP300-associated H3K27ac loci had chromatin features of transcriptional regulatory regions, we used luciferase reporter assays to measure the transcriptional activity of 1- to 2-kb regions centered on 38 dynamic EP300-associated H3K27ac loci. An equal number of loci were arbitrarily selected from each cluster, and tested regions were further subdivided into those located in promoter or nonpromoter regions. After reporter plasmid transfection, HUVECs were treated with VEGFA or vehicle. Luciferase activity measurements showed that dynamic, EP300-associated H3K27ac regions belonging to H1 and H4-12 clusters activated transcription in response to VEGFA, while regions from the H0 cluster did not (Fig. 5C,D). Regions belonging to the H1 cluster activated luciferase expression by 4 h, and expression then returned to baseline levels at 12 h. In contrast, regions from the H4-12 cluster increased luciferase activity at 4 h and maintained this through 12 h. Regions from promoter and nonpromoter regions behaved similarly (Fig. 5C,D). These data indicate that regions in H1 and H4-12 clusters function as VEGFA-responsive transcriptional enhancers, while those in the H0 cluster with decreasing H3K27ac signal did not. Together, the DNase hypersensitivity, eRNA, and luciferase assays support VEGFA-responsive transcriptional enhancer activity of dynamic, EP300-associated H3K27ac regions.

We next investigated the relationship of dynamic, EP300-associated H3K27ac loci to gene expression. We profiled gene transcript levels at 0, 1, 4, and 12 h after VEGFA stimulation by RNA-seq (Supplemental Fig. 11A). As expected, gene expression was highly dynamic following VEGFA stimulation, with 495 genes differentially expressed in at least one time point (Q-value < 0.05) (Supplemental Fig. 11A; Supplemental Table 4.). The RNA-seq data was validated by qRT-PCR and was generally concordant with previously reported microarray gene expression profiling data for HUVECs stimulated with VEGFA for 0 and 1 h (Supplemental Fig. 11B,C; Schweighofer et al. 2009) and ENCODE HUVEC RNA-seq data (Supplemental Fig. 12). To evaluate the effect of the dynamic H3K27ac loci on VEGFA-regulated gene expression, we examined expression of genes that were differentially expressed and within 100 kb of dynamic, EP300-associated H3K27ac sites (Fig. 6A). For genes associated with the H1 cluster, transcript levels were significantly higher at 1 and 4 h compared to 0 h, and returned to baseline by 12 h. For genes associated with the H4-12 cluster, expression increased by 1 h, became further increased by 4 h, and was sustained through 12 h. Expression of H0-associated genes was slightly but significantly increased at 1 h but returned to baseline levels at 4 and 12 h. Thus, each cluster of H3K27ac variation was associated with a corresponding temporal pattern of altered gene expression. These data further support the activity of the dynamic H3K27ac loci in the H1 and H4-12 clusters as transcriptional enhancers.

Dynamic H3K27sites and EP300 participate in VEGFA-stimulated chromatin looping

Enhancers are thought to stimulate transcription from promoters by forming chromatin loops (Tolhuis et al. 2002). We investigated whether VEGFA rapidly stimulated chromatin looping at dynamic, EP300-associated H3K27ac loci. The Mediator complex has been implicated in the formation of chromatin loops (Kagey et al. 2010). *MED1* and *MED12*, encoding Mediator complex subunits, were highly expressed in HUVECs (Supplemental Fig. 13A). We measured MED1 and MED12 occupancy of dynamic, EP300-associated H3K27ac sites by ChIP-qPCR (Fig. 6B; Supplemental Fig. 13B–E). At seven of eight loci belonging to cluster H1, MED1 and MED12 enrichment strongly increased at 1 h of VEGFA treatment, then declined to basal levels at 4 to 12 h. In cluster H4-12, MED1 and MED12 were enriched at most loci, but the degree of enrichment did not change in a consistent temporal pattern following VEGFA treatment. These results indicate that the Mediator complex is

bound to dynamic, EP300-associated H3K27ac sites and suggest that these sites may undergo VEGFA-stimulated looping.

To directly test the hypothesis that dynamic, EP300-associated H3K27ac sites loop into proximity with promoters after VEGFA stimulation, we used chromatin conformation capture (Dekker et al. 2002) to study temporal changes in chromatin conformation involving three loci with VEGFA-stimulated increases in H3K27ac. Upstream of *DUSP5*, a dynamic H3K27ac site belonging to cluster H1 became transiently associated with the promoter at 1 h (Fig. 7), when it was maximally occupied by H3K27ac, EP300, and MED1/12, and maximally transcribed as eRNA. At later time points, the association of these regions declined, coincident with decreased EP300 and MED1/12 occupancy, and decreased eRNA transcription. Upstream of *KDR* (encoding VEGFR2, a VEGFA receptor), dynamic H3K27ac sites belonging to cluster H4-12 became associated with the promoter within 1 h of VEGFA stimulation (Fig. 7). This correlated with its time course of EP300 and MED1/12 occupancy and eRNA transcription but preceded its maximal occupancy by H3K27ac. Similar observations were made at a second dynamic H3K27ac site from cluster H4-12 located upstream of the endothelial gene *CD34* (Fig. 7). Thus, at these sites, VEGFA stimulation rapidly altered chromatin conformation and stimulated eRNA transcription, and these events preceded deposition of H3K27ac.

To probe the requirement of EP300 in chromatin looping, we repeated the chromatin conformation capture experiments in the presence of the EP300 inhibitor C646 (Fig. 7). C646 blocked VEGFA-stimulated chromatin looping, thereby establishing the importance of EP300 in establishing chromatin loops. Consistent with a key role of EP300 acetyltransferase activity in mediating VEGFA-stimulated chromatin changes and activation of gene transcription, C646 potently blocked up-regulation of genes normally induced by VEGFA, including *DUSP5*, *KDR*, *NR4A1*, and *CD34* (Fig. 7E).

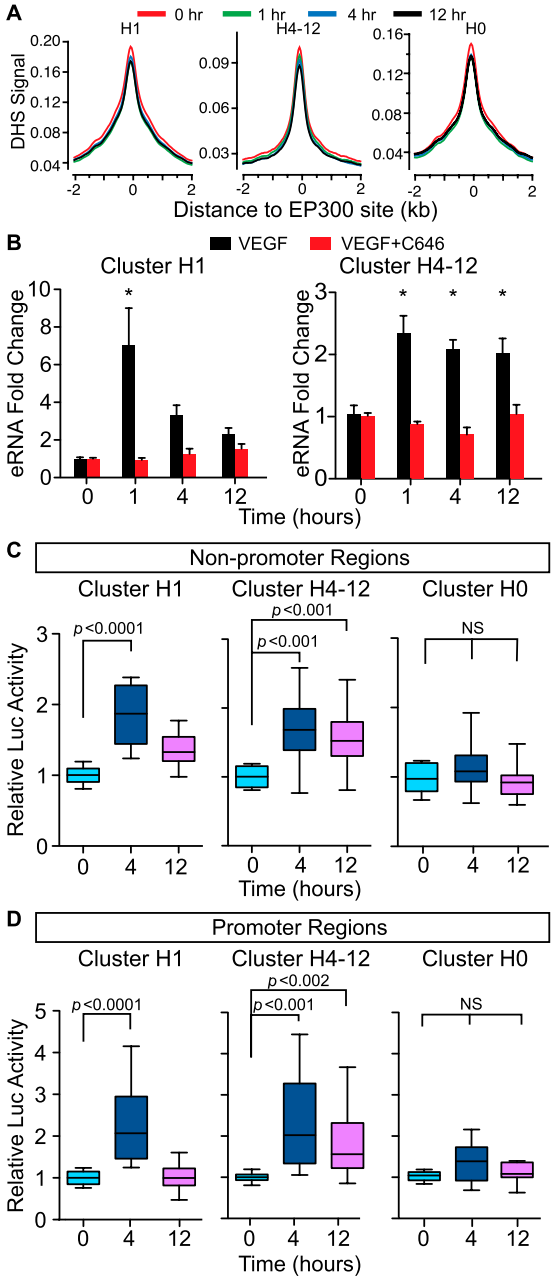

Figure 5. Dynamic H3K27ac regions had functional properties of transcriptional regulatory regions. (*A*) DNase-seq showed that dynamic, EP300-associated sites are hypersensitive to DNase I digestion, but the sensitivity did not change substantially during the VEGFA stimulation time course. DNase signal is plotted as reads per 10^{-6} mapped reads. (*B*) eRNA expression from dynamic H3K27ac regions with or without EP300 inhibition by C646. Each bar represents the average of 5–6 different regions (individual data are shown in Supplemental Fig. 7). (*) $P < 0.05$. (*C*,*D*) Luciferase activity of dynamic H3K27ac regions at promoter and non-promoter sites. Luciferase activity was expressed relative to the activity measured at time 0. $n = 5$–8 per group. Line, bar, and whiskers represent median, quartiles, and min-max values, respectively.

Discussion

Epigenetic signatures define transcriptional regulatory elements that underlie the distinct gene expression programs of different cell types, and these signatures have been used to annotate cell type-specific functional elements (Heintzman et al. 2007; Ernst et al. 2011; Kharchenko et al. 2011; Bonn et al. 2012). However, less is known about how the chromatin landscape responds to transient environmental cues. To gain insights into this area, we studied changes in H3K27 acetylation that occur within 12 h of endothelial cell stimulation with VEGFA, a major regulator of angiogenesis. We showed that VEGFA induces rapid changes in H3K27ac at thousands of genomic loci. We demonstrated that dynamic changes in H3K27ac define VEGFA-regulated transcriptional regulatory elements. These regions had characteristics of activity-regulated enhancers: they were tightly linked to EP300 chromatin occupancy, had functional annotations linked to blood vessel development, were transcribed as VEGFA-stimulated eRNAs, and engaged in VEGFA-regulated chromatin looping and gene expression. These regions with dynamic H3K27ac exhibited VEGFA-stimulated transcriptional activity in both luciferase assays and in HUVEC gene expression profiles, and EP300 inhibition blocked VEGFA-induced changes in H3K27ac and gene expression. Thus, our study indicates that the epigenome is an integral participant in signal-induced transcriptional responses.

We developed a novel epigenetic signature based on the signal-induced variation of H3K27ac chromatin occupancy. Using this signature, we identified thousands of novel endothelial, VEGFA-responsive transcriptional regulatory elements and the transcription factor families that are likely to regulate them. These

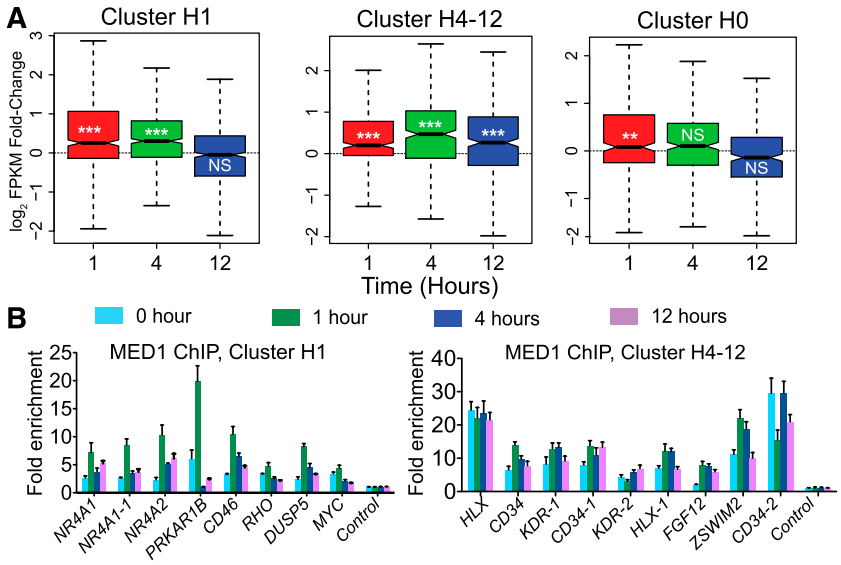

Figure 6. VEGFA-increased gene expression and mediator binding associated with dynamic H3K27ac loci in H1 and H4-12 clusters. (*A*) Fold change of differentially expressed genes within 100 kb of dynamic H3K27ac loci belonging to the indicated clusters, compared to 0 h. Line, boxes, and whiskers are as in Fig. 5A,B. Notches are a function of the interquartile difference and inversely related to the square root of the sample size. (***) $P < 0.0001$, (**) $P < 0.001$. (NS) Not significant. (*B*) MED1 ChIP-qPCR of dynamic H3K27ac loci belonging to H1 or H4-12 clusters.

regulatory elements were associated with genes that regulate angiogenesis and could be separated into distinct functional groups based upon their temporal variation of H3K27 acetylation. These data will provide an important resource for future studies of the transcriptional regulation of angiogenesis, although we note that this study was performed in cultured venous endothelial cells and that other VEGFA-responsive endothelial enhancers active in other endothelial cell types or active in vivo were likely not detected in this system. More broadly, we anticipate that application of our epigenetic signature based upon signal-induced chromatin feature variation to other biological systems will enhance annotation of activity-regulated functional elements genome-wide.

Previous studies suggested that nucleosome dynamics define activity-regulated transcriptional enhancers (He et al. 2010; Bonn et al. 2012). However, our data suggest that rapid changes in H3K27ac were not due to changes in chromatin accessibility/nucleosome occupancy. Rather, dynamic H3K27 acetylation was closely associated with EP300, and, indeed, EP300 and its acetyltransferase activity were required to write these marks. These data indicate that epigenetic enzymatic activity is also an important factor that establishes activity-regulated transcriptional enhancers.

Our experiments highlight the crucial role of EP300 in mediating signal-responsive changes in H3K27ac and gene expression. EP300 is a histone acetyltransferase that was previously reported to occupy tissue-specific transcriptional enhancers (Visel et al. 2009). Our data show the proximity of regions occupied by EP300 and regions with VEGFA-stimulated variation in H3K27ac. Inhibition of VEGFA-induced H3K27ac accumulation by EP300 antagonists supports the causal role of EP300 in dynamic variation of H3K27ac occupancy. Furthermore, EP300 inhibition dramatically blocked gene expression changes induced by VEGFA. These data directly demonstrate the key role of EP300 in executing VEGFA-induced transcriptional responses and suggest more broadly that EP300 is required for signal-induced changes in histone acetylation and gene expression.

To identify transcription factors that participate in the VEGFA transcriptional response and recruit EP300 to dynamic H3K27ac sites, we found transcription factor motifs enriched in EP300-bound regions. ETS, FOX, AP1, and STAT transcription factor motifs were enriched in all three clusters, suggesting that members of these transcription factor families broadly participate in VEGFA-driven transcriptional changes. The key role of several ETS factors in angiogenesis was reviewed recently (Randi et al. 2009). We directly confirmed ETS1 occupancy of most EP300-bound regions, validating the motif analysis and providing a resource for further study of the role of ETS1 in angiogenesis and VEGFA-induced gene expression changes. The extensive overlap between EP300 and ETS1 binding suggests that ETS1 may contribute to EP300 recruitment. Consistent with this hypothesis, ETS1 knockdown blocked VEGFA-induced H3K27ac changes at ETS1-bound loci. Compared to ETS, relatively less is known about the role of FOX, AP1, and STAT transcription factor family members as effectors of VEGFA signaling. Our data identify regions potentially regulated by these factors downstream from VEGFA. Recently, FOX transcription factors were reported to interact with ETS factors to regulate vasculogenesis, and similar interactions may also contribute to angiogenesis (De Val et al. 2008). Our data also indicate that AP1 is an important transcriptional effector of VEGFA. Although this role of AP1 has not been studied, AP1 is well-positioned in intracellular signaling pathways to act in this capacity: AP1 is a major nuclear target of MAPK signaling, which is robustly activated downstream from VEGFA (D'Angelo et al. 1995).

We also identified transcription factor motifs that were enriched in a subset of dynamic H3K27ac clusters, suggesting a link to specific temporal patterns of H3K27 acetylation and to specific functional pathways. In the early-responding H1 cluster, we detected significant enrichment for the ATF1/CREB1 (activating transcription factor 1 and cyclic-AMP response element binding protein 1) motifs (Fig. 4D; Supplemental Table 3). These transcription factors mediate immediate early responses, which predominate the functional terms linked to the H1 cluster. GATA and TEAD motifs were overrepresented in the H4-12 and H0 clusters. GATA2 has been implicated as a key regulator of endothelial gene transcription (Linnemann et al. 2011), and Tead4 (also known as RTEF-1 and TEF-3) was recently reported to be required for VEGFA-stimulated angiogenesis (Liu et al. 2011). GATA2 and Tead4 likely contribute to endothelial cell-specific functional term enrichment in the H4-12 and H0 clusters. GATA factors are also crucial in regulating hematopoiesis. However, GO terms related to blood development were not overrepresented in the H4-12 or H0 cluster, suggesting that the GATA motifs identified by our analysis are selectively active in endothelial cells. The H0 and H1 clusters, which share a decline of H3K27ac at 4–12 h, were both enriched for the binding motif of RBP/J, the nuclear target of Notch signaling. Interestingly, VEGFA signaling activates the Notch pathway, which, in turn, antagonizes VEGFA action in an auto-regulatory loop (Hellstrom et al. 2007; Holderfield and Hughes 2008). Collectively,

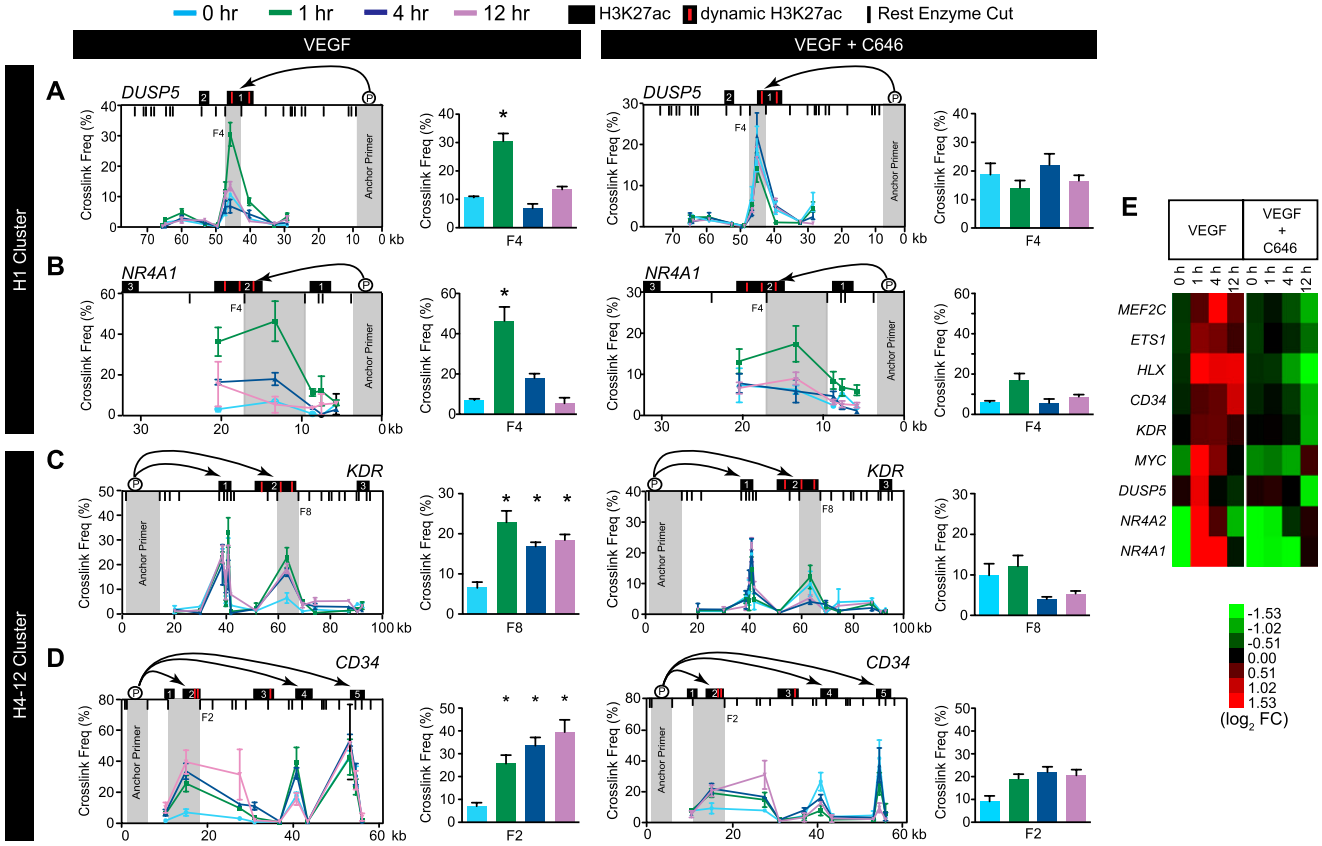

Figure 7. Promoter contact with dynamic H3K27ac loci in H1 and H4-12 clusters was stimulated by VEGFA and required EP300 activity. (*A–D*) Chromatin confirmation capture of dynamic H3K27ac sites (red lines) near *DUSP5*, *NR4A1*, *KDR*, and *CD34*. (Black boxes) Regions of H3K27ac enrichment; chromatin looping was attenuated by pretreatment of HUVEC cells with C646 for 30 min. (Red lines) Dynamic H3K27ac sites. (Gray bars) Promoter anchor primers and fragments graphed to the *right*. (Vertical black lines) Cutting sites of restriction enzyme used for chromatin conformation capture. (*) $P < 0.05$. (*E*) EP300 acetyltransferase activity was required for activation of gene expression downstream from VEGFA. Gene expression was measured by qRT-PCR during VEGFA stimulation in the presence or absence of the EP300 inhibitor C646.

these data suggest that distinct transcription factor families contribute to the different temporal and functional properties of the H0, H1, and H4-12 clusters.

In addition to its role in depositing H3K27ac, EP300 catalytic activity was required for VEGFA-induced chromatin looping. To our knowledge, the requirement of EP300 in chromatin looping has not been reported previously. Furthermore, the time course data, surprisingly, suggest that, for members of the H4-12 cluster, eRNA expression and chromatin looping occur prior to up-regulation of H3K27ac, yet are dependent on EP300 catalytic activity. Further work is required to establish the mechanism(s) through which EP300 acetyltransferase activity promotes eRNA expression and chromatin looping and how the interplay between these chromatin properties regulates gene transcription.

Methods

Detailed descriptions of cell culture, ChIP-seq, RNA-seq, DNase-seq, chromatin conformation capture, luciferase assays, and their integrative analysis are provided in the Supplemental Material. Primary HUVEC cells were cultured overnight in EBM2 with 0.5% FBS, then treated with 50 μg/mL VEGFA for 0, 1, 4, and 12 h. Chromatin occupancy analysis was performed by ChIP-seq and ChIP-qPCR following established protocols (Lee et al. 2006), with minor modifications. Antibodies are listed in Supplemental Table 5. Polyadenylated RNA expression was profiled by mRNA-seq as described (Christodoulou et al. 2011), with minor modifications. DNase-seq was performed as described (Song and Crawford 2010), with modifications to library construction to permit multiplex sequencing. Chromatin conformation capture was performed as described (Hagege et al. 2007). Luciferase assays were performed using 1–2 kb genomic regions cloned upstream of luciferase. Primers used in this study are listed in Supplemental Table 6.

ChIP-seq and DNase-seq reads were mapped with Bowtie (Langmead et al. 2009) (summarized in Supplemental Table 5). EP300 peaks were called using SPP (Kharchenko et al. 2008). DNase-seq peaks were called using F-seq as described (Boyle et al. 2008). H3K27ac ChIP-seq enrichment over input in 200-bp windows, tiled at 50-bp intervals, were calculated across the genome. The H3K27ac variance score for each window was calculated as $\log_2$ of the variance of H3K27ac in the window over time, divided by the mean of H3K27ac in the window. Windows with low mean signal were discarded. For each EP300 site, we identified the H3K27ac region within 2 kb with greatest variance score. Of these regions, the top 20th percentile was defined as dynamic, EP300-associate H3K27ac regions. RNA-seq and differential expression analysis was performed using Cufflinks and

Cuffdiff (Trapnell et al. 2010). Motif discovery was performed using DREME (Bailey 2011), and motifs were annotated with TomTom (Gupta et al. 2007).

Data access

All sequencing data were deposited in the NCBI Gene Expression Omnibus (GEO) (http://www.ncbi.nlm.nih.gov/geo/) under accession number GSE41166. The data are also available through the Cardiovascular Development Consortium at https://b2b.hci.utah.edu/gnomex/.

Acknowledgments

W.T.P. was supported by an American Heart Association Established Investigator Award and National Heart, Lung, and Blood Institute award U01HL098166, and by charitable contributions from Karen Carpenter, Edward Marram, and Gail Federici Smith. The content is solely the responsibility of the authors and does not necessarily represent the official views of the National Heart, Lung, and Blood Institute or the National Institutes of Health.

Author contributions: B.Z. and W.T.P. designed the experiments. B.Z. and J.C. executed the experiments. L.S. and G.E.C. performed DNase-seq experiments. D.C. and J.G.S. assisted with RNase-seq experiments. B.Z., D.S.D., J.H., P.J.P., and W.T.P. analyzed the data. B.Z., D.S.D., and W.T.P. wrote the manuscript.

References

Altarejos JY, Montminy M. 2011. CREB and the CRTC co-activators: Sensors for hormonal and metabolic signals. *Nat Rev Mol Cell Biol* **12:** 141–151.

Bailey TL. 2011. DREME: Motif discovery in transcription factor ChIP-seq data. *Bioinformatics* **27:** 1653–1659.

Bonn S, Zinzen RP, Girardot C, Gustafson EH, Perez-Gonzalez A, Delhomme N, Ghavi-Helm Y, Wilczynski B, Riddell A, Furlong EE. 2012. Tissue-specific analysis of chromatin state identifies temporal signatures of enhancer activity during embryonic development. *Nat Genet* **44:** 148–156.

Bowers EM, Yan G, Mukherjee C, Orry A, Wang L, Holbert MA, Crump NT, Hazzalin CA, Liszczak G, Yuan H, et al. 2010. Virtual ligand screening of the p300/CBP histone acetyltransferase: Identification of a selective small molecule inhibitor. *Chem Biol* **17:** 471–482.

Boyle AP, Davis S, Shulha HP, Meltzer P, Margulies EH, Weng Z, Furey TS, Crawford GE. 2008. High-resolution mapping and characterization of open chromatin across the genome. *Cell* **132:** 311–322.

Carmeliet P, Jain RK. 2011. Molecular mechanisms and clinical applications of angiogenesis. *Nature* **473:** 298–307.

Christodoulou DC, Gorham JM, Herman DS, Seidman JG. 2011. Construction of normalized RNA-seq libraries for next-generation sequencing using the crab duplex-specific nuclease. *Curr Protoc Mol Biol* **94:** 4.12.1–4.12.11.

Creyghton MP, Cheng AW, Welstead GG, Kooistra T, Carey BW, Steine EJ, Hanna J, Lodato MA, Frampton GM, Sharp PA, et al. 2010. Histone H3K27ac separates active from poised enhancers and predicts developmental state. *Proc Natl Acad Sci* **107:** 21931–21936.

D'Angelo G, Struman I, Martial J, Weiner RI. 1995. Activation of mitogen-activated protein kinases by vascular endothelial growth factor and basic fibroblast growth factor in capillary endothelial cells is inhibited by the antiangiogenic factor 16-kDa N-terminal fragment of prolactin. *Proc Natl Acad Sci* **92:** 6374–6378.

De Val S, Chi NC, Meadows SM, Minovitsky S, Anderson JP, Harris IS, Ehlers ML, Agarwal P, Visel A, Xu SM, et al. 2008. Combinatorial regulation of endothelial gene expression by ets and forkhead transcription factors. *Cell* **135:** 1053–1064.

Dekker J, Rippe K, Dekker M, Kleckner N. 2002. Capturing chromosome conformation. *Science* **295:** 1306–1311.

Ernst J, Kheradpour P, Mikkelsen TJ, Shoresh N, Ward LD, Epstein CB, Zhang X, Wang L, Issner R, Coyne M, et al. 2011. Mapping and analysis of chromatin state dynamics in nine human cell types. *Nature* **473:** 43–49.

Gupta S, Stamatoyannopoulos JA, Bailey TL, Noble WS. 2007. Quantifying similarity between motifs. *Genome Biol* **8:** R24.

Hagege H, Klous P, Braem C, Splinter E, Dekker J, Cathala G, de Laat W, Forne T. 2007. Quantitative analysis of chromosome conformation capture assays (3C-qPCR). *Nat Protoc* **2:** 1722–1733.

He HH, Meyer CA, Shin H, Bailey ST, Wei G, Wang Q, Zhang Y, Xu K, Ni M, Lupien M, et al. 2010. Nucleosome dynamics define transcriptional enhancers. *Nat Genet* **42:** 343–347.

Heintzman ND, Stuart RK, Hon G, Fu Y, Ching CW, Hawkins RD, Barrera LO, Van Calcar S, Qu C, Ching KA, et al. 2007. Distinct and predictive chromatin signatures of transcriptional promoters and enhancers in the human genome. *Nat Genet* **39:** 311–318.

Hellstrom M, Phng LK, Gerhardt H. 2007. VEGF and Notch signaling: The yin and yang of angiogenic sprouting. *Cell Adhes Migr* **1:** 133–136.

Holderfield MT, Hughes CC. 2008. Crosstalk between vascular endothelial growth factor, notch, and transforming growth factor-β in vascular morphogenesis. *Circ Res* **102:** 637–652.

Kagey MH, Newman JJ, Bilodeau S, Zhan Y, Orlando DA, van Berkum NL, Ebmeier CC, Goossens J, Rahl PB, Levine SS, et al. 2010. Mediator and cohesin connect gene expression and chromatin architecture. *Nature* **467:** 430–435.

Kharchenko PV, Tolstorukov MY, Park PJ. 2008. Design and analysis of ChIP-seq experiments for DNA-binding proteins. *Nat Biotechnol* **26:** 1351–1359.

Kharchenko PV, Alekseyenko AA, Schwartz YB, Minoda A, Riddle NC, Ernst J, Sabo PJ, Larschan E, Gorchakov AA, Gu T, et al. 2011. Comprehensive analysis of the chromatin landscape in *Drosophila melanogaster*. *Nature* **471:** 480–485.

Kim TK, Hemberg M, Gray JM, Costa AM, Bear DM, Wu J, Harmin DA, Laptewicz M, Barbara-Haley K, Kuersten S, et al. 2010. Widespread transcription at neuronal activity-regulated enhancers. *Nature* **465:** 182–187.

Kundaje A, Kyriazopoulou-Panagiotopoulou S, Libbrecht M, Smith CL, Raha D, Winters EE, Johnson SM, Snyder M, Batzoglou S, Sidow A. 2012. Ubiquitous heterogeneity and asymmetry of the chromatin environment at regulatory elements. *Genome Res* **22:** 1735–1747.

Langmead B, Trapnell C, Pop M, Salzberg SL. 2009. Ultrafast and memory-efficient alignment of short DNA sequences to the human genome. *Genome Biol* **10:** R25.

Lee TI, Johnstone SE, Young RA. 2006. Chromatin immunoprecipitation and microarray-based analysis of protein location. *Nat Protoc* **1:** 729–748.

Linnemann AK, O'Geen H, Keles S, Farnham PJ, Bresnick EH. 2011. Genetic framework for GATA factor function in vascular biology. *Proc Natl Acad Sci* **108:** 13641–13646.

Liu X, Zhao D, James L, Li J, Zeng H. 2011. Requirement of the nuclear localization of transcription enhancer factor 3 for proliferation, migration, tube formation, and angiogenesis induced by vascular endothelial growth factor. *FASEB J* **25:** 1188–1197.

Ogryzko VV, Schiltz RL, Russanova V, Howard BH, Nakatani Y. 1996. The transcriptional coactivators p300 and CBP are histone acetyltransferases. *Cell* **87:** 953–959.

Rada-Iglesias A, Bajpai R, Swigut T, Brugmann SA, Flynn RA, Wysocka J. 2011. A unique chromatin signature uncovers early developmental enhancers in humans. *Nature* **470:** 279–283.

Randi AM, Sperone A, Dryden NH, Birdsey GM. 2009. Regulation of angiogenesis by ETS transcription factors. *Biochem Soc Trans* **37:** 1248–1253.

Reddy TE, Gertz J, Pauli F, Kucera KS, Varley KE, Newberry KM, Marinov GK, Mortazavi A, Williams BA, Song L, et al. 2012. Effects of sequence variation on differential allelic transcription factor occupancy and gene expression. *Genome Res* **22:** 860–869.

Schweighofer B, Testori J, Sturtzel C, Sattler S, Mayer H, Wagner O, Bilban M, Hofer E. 2009. The VEGF-induced transcriptional response comprises gene clusters at the crossroad of angiogenesis and inflammation. *Thromb Haemost* **102:** 544–554.

Song L, Crawford GE. 2010. DNase-seq: A high-resolution technique for mapping active gene regulatory elements across the genome from mammalian cells. *Cold Spring Harb Protoc* doi: 10.1101/pdb.prot5384.

Tolhuis B, Palstra RJ, Splinter E, Grosveld F, de Laat W. 2002. Looping and interaction between hypersensitive sites in the active β-globin locus. *Mol Cell* **10:** 1453–1465.

Trapnell C, Williams BA, Pertea G, Mortazavi A, Kwan G, van Baren MJ, Salzberg SL, Wold BJ, Pachter L. 2010. Transcript assembly and quantification by RNA-Seq reveals unannotated transcripts and isoform switching during cell differentiation. *Nat Biotechnol* **28:** 511–515.

Visel A, Blow MJ, Li Z, Zhang T, Akiyama JA, Holt A, Plajzer-Frick I, Shoukry M, Wright C, Chen F, et al. 2009. ChIP-seq accurately predicts tissue-specific activity of enhancers. *Nature* **457:** 854–858.

Wang D, Garcia-Bassets I, Benner C, Li W, Su X, Zhou Y, Qiu J, Liu W, Kaikkonen MU, Ohgi KA, et al. 2011. Reprogramming transcription by distinct classes of enhancers functionally defined by eRNA. *Nature* **474:** 390–394.

Xi H, Shulha HP, Lin JM, Vales TR, Fu Y, Bodine DM, McKay RDG, Chenoweth JG, Tesar PJ, Furey TS, et al. 2007. Identification and characterization of cell type-specific and ubiquitous chromatin regulatory structures in the human genome. *PLoS Genet* **3:** e136.

Zentner GE, Tesar PJ, Scacheri PC. 2011. Epigenetic signatures distinguish multiple classes of enhancers with distinct cellular functions. *Genome Res* **21:** 1273–1283.

Received September 22, 2012; accepted in revised form March 29, 2013.

Supplementary Information

Table of Contents:

Materials and Methods

Cell culture

Primary HUVEC cells (Lonza) were cultured in full EGM2 media. For time course experiments, cells at less than six passages were cultured overnight in EGM2 with 0.5% FBS and then stimulated with 50 μg/ml VEGF (R&D Systems) for 0, 1, 4 and 12 hours. For siRNA transfection, EP300 or control siRNAs (Suppl. Table 4) were transfected into HUVEC cells using siLentFectTM Lipid (Bio-Rad). Experiments were performed 48 hours after siRNA transfection. C646 (Calbiochem) was added to cells at 10 μg/ml 30min before addition of VEGF.

Chromatin immunoprecipitation:

HUVEC cells were crosslinked with 1% formaldehyde for 10 min at room temperature. Crosslinking was stopped by glycine to 0.125 M. Subsequent steps for chromatin preparation were performed at 4°C as described previously(Lee et al. 2006), with modifications. Nuclei from 5 x 10^7 cells were extracted with nuclear extraction buffer (20 mM Hepes-KOH pH 7.5, 10 mM KCl, 1 mM EDTA, 0.2% NP40, 1 mM DTT and 10% glycerol) and resuspended in 1 ml sonication buffer (20 mM Tris-HCl pH 8, 150 mM NaCl, 2 mM EDTA, 0.1% SDS, 1% Triton X-100). The extracted nuclei were sonicated using a Misonix Sonicator 3000 (28 cycles, consisting of a 15 second pulse at amplitude 70 followed by 1 min rest). After sonication, insoluble material was removed by centrifugation at 12000xg for 15 min.

Chromatin immunoprecipitation was performed by incubating sonicated chromatin, pre-cleared with 50 µl proteinase A dynabeads (Invitrogen), with 10 µg ChIP antibodies (Suppl. Table 3) overnight at 4°C. Next, antibody-bound chromatin was pulled down using 100 µl BSA-blocked Proteinase A or G dynabeads were added to each sample (A or G were selected based on the antibody species of origin). Beads were washed five times with RIPA buffer (50 mM Hepes-KOH pH 7.5, 500 mM LiCl, 1 mM EDTA, 1% NP40 and 0.7% Na-Deoxycholate) using a magnetic stand. For MED1 and MED12 ChIP, protein G dynabeads were washed once with sonication buffer, once with high salt buffer (20 mM Tris-HCl pH 8, 500 mM NaCl, 2 mM EDTA, 0.1%, SDS, 1% Triton X-100), once with LiCl Buffer (10 mM Tris-HCl pH 8, 250 nM LiCl, 2mM EDTA, 1% NP40) and once with 10mM Tris-HCl pH 8, 10 mM EDTA, and 50 mM NaCl. Precipitated DNA was de-crosslinked at 65°C overnight, treated with 10 µg RNase A and 15 µg proteinase K, and then purified using the Qiagen Min-elute PCR Purification kit.

Chip-qPCR

ChIP and input DNA sample were amplified with SYBR@ master mix (Life Technologies, USA) on an ABI7500 cycler. ChIP enrichment was calculated by normalization with input and unbound control regions as described previously (He and Pu 2010). Primers used for ChIP-qPCR are listed in Suppl. Table 4. Primers for validation of MED1/12 ChIP in murine ES cells were described previously(Kagey et al. 2010).

ChIP-seq

Chip-Seq library construction were performed with NEBNext DNA Sample Prep Reagent Set 1 (E6000) using the protocol and reagent concentrations described in the Illumina Mutiplex ChIP-Seq DNA Sample Prep Kit. Libraries were indexed using a single indexed PCR primer (Suppl. Table 4) in place of the dual multiplex Primer 2.0/indexed primers described in the final PCR step of the Illumina protocol. ChIP library size was checked by using an Agilent bioanalyzer, and the functional cluster concentration of each library was determined by qPCR. Libraries were sequenced using a HiSeq 2000 (Illumina) instrument to generate 50 nt single end data. ChIP-seq data for GM12878 were from obtained from wgEncodeEH001487; ref. _(Reddy et al. 2012).

mRNA-seq

Total RNA of VEGF-treated and non-treated HUVEC cells were isolated with the Qiagen RNeasy mini kit, including on column DNaseI digestion. mRNA selection and library construction was performed as described (Christodoulou et al. 2011), without the library normalization steps. The final PCR amplification was performed with the indexing primers listed in Suppl. Table 4 in place of the dual PCR primer 2.0/indexing primers described in the published protocol. Pair-end, 50 nt sequences were generated on a HiSeq 2000 (Illumina).

DNase-seq

DNase-seq was performed as described previously (Song and Crawford 2010), with minor modification to permit multiplexing. $3X10^7$ HUVEC cells were collected at 0, 1, 4 and 12 hour after VEGF stimulation, washed with cold PBS, suspended into FBS with 10% DMSO, and stored at -80°C prior to subsequent processing. For DNase digestion, nuclei were isolated from thawed cells and treated with DNase I as described(Song and Crawford 2010). DNA nicks were end repaired and ligated with biotin-labeled DNS linker 1. MmeI digestion released 20bp chromatin DNA afixed to the biotinylated primer. These fragments were purified with streptavidin dynabead. DNA linker 2 with barcode (Suppl. Table 4) was ligated to purified fragments, and the sequencing library was amplified with high fidelity PCR. Libraries were sequenced on an Illumina HiSeq 2000 (50 nt, single end) using a custom library sequencing primer (Suppl. Table 4). Duplicate samples showed high correlation, and replicate 1 was used for the main analysis.

Immunoprecipitation and Western Blotting

To pull down mediator proteins in the HUVEC and murine ES cells, 1 mg soluble protein was incubated with 3 µg MED1 or MED12 antibody (Suppl. Table 3) overnight at 4 °C. Antibody complexes were then pulled down on Protein A dynabeads, pre-blocked with 1% BSA, for 4 hours at 4°C. After washing, proteins were eluted in 1X Laemmli buffer. Western blotting was performed using standard methods.

Chromatin Conformation Capture (3C)

Chromatin Conformation Capture was performed essentially as described(Hagege et al. 2007; Xu et al. 2010). $1x10^7$ HUVEC cells treated with 50 µg/ml VEGF for 0, 1, 4 and 12 hours were crosslinked with 2% formaldehyde for 8 min at room temperature on dish. Nuclei were extracted with nuclear extraction buffer and digested with 1000 U EcoRI overnight on a shaking platform. The digested nuclei were ligated with 100 Weiss units of T4 ligase at 16°C for 4 hours in 7 ml 1X ligation buffer. Digestion efficiency was measured using quantitative PCR to compare aliquots taken before and after digestion. Samples with less than 70% complete digestion were discarded. BAC clones (20 µg) containing *KDR* (Invitrogen, clone CTD-2506A13), *CD34* (CHORI, clone RP11-351B8), *DUSP5* (CHORI, clone RP11-108I5) and *VWF* (CHORI, clone RP11-1137J12) were digested with EcoRI and religated to generate control template. Ligation products were measured by quantitative Taqman PCR using primers and probes indicated in Suppl. Table 4. Normalized crosslink frequency was calculated as described(Hagege et al. 2007).

Enhancer/promoter transcriptional activity assay

1-2 kb regions centered on EP300 binding sites nearest H3K27ac dynamic regions were amplified with *LA Taq* DNA Polymerase (Takara) and inserted into pGL4.11[luc2P] (promoter) or pGL4.24[luc2P/minP] (Enhancer) vectors (Promega, USA) by Gateway recombination (Invitrogen). HUVEC seeded on 24 well plates were then cotransfected with luciferase reporter and internal control (pGL4.74[hRluc/TK] (Promega, USA) plasmids using Lipofectamine LTX (Invitrogen, USA). One day after transfection, cells were serum-depleted overnight and then stimulated with VEGF. Luciferase activity was measured using a 1420 Multilabel Counter (PerkinElmer, USA) after adding Dual-Luciferase Assay substrate (Promega, USA).

Data Analysis

ChIP-seq and DNase-seq Read Alignment. All samples were aligned against hg19 using Bowtie 1.3(Langmead et al. 2009) with the –m 1 switch to only recover uniquely mapping reads. Each set of aligned reads were read into R via the package SPP(Kharchenko et al. 2008) and then filtered for quality using the function remove.local.tag.anomalies. All analyses below were then performed on the filtered read set .

EP300 Peak Calls. Using SPP(Kharchenko et al. 2008) on the processed EP300 ChIP-seq data (rep 1), peaks were called using find.binding.positions with a window half size of 120 and a FDR of 1%.

H3K27ac variance scores and temporal clusters. To calculate H3K27ac variance scores, the entire genome was divided into 200 bp windows at 50 bp intervals. At each time point, H3K27ac reads were shifted by 73 bp and mapped to bins. For bins containing at least one read, the enrichment was calculated by normalizing it against similarly binned input. The variance score of each bin was calculated as variance(bins over time)/mean (bins over time). A EP300-associated H3K27ac site was defined as the bin ± 2kb from the center of a EP300 site that had the greatest variance score and a mean value of greater than or equal to 3. The subset of EP300-associated H3K27ac with highest variance scores (top 20 percentile) were defined as dynamic, EP300-associated H3K27ac sites and were used for further analysis.

H3K27ac clusters were determined using the dynamic, EP300-associated H3K27ac sites. The variance score of each site was row-scaled across time using a standard normal distribution, then grouped by Hierarchical clustering with average linkage and Ward's method. The top three clusters from the resulting dendrogram were designated H1, H4-12, and H0 based on the temporal pattern of H3K27ac variance score (Suppl. Table 1).

Functional strand clustering. To assess whether the H3K27ac and p300 had asymmetric patterns around our variant peak centers, we carried out the functional strand clustering method as described by Kundaje et al. (2012), with some modifications. For each variant cluster, we took the tag density matrix around H3K27ac peaks for both H3K27ac and p300 signal across all four time points. In order to capture patterns across time points and factors, we joined the

H3K27ac and p300 matrixes so that each row represented these signals in the 4 kb centered on the variant site center, across all 4 time points. After creating this joint matrix, we filtered out rows that had a mean signal in the 1st percentile of all rows. After this filtering, we clustered the matrix with k-means clustering, starting with 40 clusters. We then progressively merged similar clusters by their Pearson correlation distance between the cluster means, calculated from all the rows in the cluster from the joint matrix. At each step, the two clusters with the value that minimized the 1-Pearson correlation were merged together. If flipping a cluster's orientation reduced the Pearson correlation distance and led to merger of two clusters, then the cluster was flipped by reversing the orientation of each constituent matrices and then rejoining them in a new joint matrix. This procedure was reiterated until no cluster had a 1-Pearson correlation value less than or equal to .25. After this process, each remaining cluster was then oriented such that the strongest mean signal in the cluster was on the right side of the image.

Assigning Functional Annotations to Dynamic, p-300 associated H3K27ac Clusters. The position of each site in the H1, H4-12, and H0 clusters was analyzed using GREAT(McLean et al. 2010). Peaks were associated with the nearest gene within 100 kb. Selected entries from the top 20 significant terms from the Biological Process table are shown in Fig. 4c.

Tag Aggregation Plots and Heatmaps. Reads within 3 kb of a feature of interest (either a EP300-associated H3K27ac site, or a peak, as indicated) were binned into 10 bp bins. The aggregation plots were generated by taking the 5% trimmed mean of each bin and normalizing against the mapped library size. For all data sets except DHS, this value was then subtracted against a similarly prepared input matrix. The resulting curve was smoothing using loess smoothing and then plotted. The tag density heatmaps were generated by producing a matrix from the 50 bp binned sites centered on H3K27ac variants, normalizing against the number of mapped reads. The matrix of normalized tag number was log2 transformed and visualized using JavaTreeView (Saldanha 2004).

mRNA-seq Analysis. The paired end RNA-seq reads were aligned to Ensembl transcript annotation using Cufflinks 1.3.0(Trapnell et al. 2010) to give gene expression values, expressed as fragments per thousand nt transcript per million reads (FPKM). Each individual RNA-seq sample was initially independently aligned against the Ensembl transcript annotation. Then Cuffdiff was used to identify differentially expressed genes. The time series option was used (-T) to direct Cuffdiff to compare a sample only against the next sample in the series. To generate the heat map of differentially expressed genes, the z-score for each differentially expressed gene was calculated across the time course. These were then clustered by hierarchical clustering using Euclidean distance and Ward's method.

DHS data analysis. DHS raw sequence reads were separated by their barcode and the adaptor sequence was removed with Btrim(Kong 2011). The reads without genomic inserts were discarded. The remain sequences were then

aligned to hg19 using Bowtie2, with Strata selected. About 70% of reads were uniquely mapped.

De novo Motif Discovery. The central 100 bp of each EP300 peak associated with a dynamic H3K27ac site was analyzed for over-represented motifs using DREME(Bailey 2011). Discovered motifs were annotated by matching to known motifs in the Jaspar(Portales-Casamar et al. 2010) and Uniprobe(Newburger and Bulyk 2009) databases using TomTom(Gupta et al. 2007).

Supplementary References

Bailey TL. 2011. DREME: motif discovery in transcription factor ChIP-seq data. *Bioinformatics* **27**: 1653-1659.

Christodoulou DC, Gorham JM, Herman DS, Seidman JG. 2011. Construction of normalized RNA-seq libraries for next-generation sequencing using the crab duplex-specific nuclease. *Curr Protoc Mol Biol* **Chapter 4**: Unit4.12.

Gupta S, Stamatoyannopoulos JA, Bailey TL, Noble WS. 2007. Quantifying similarity between motifs. *Genome Biol* **8**: R24.

Hagege H, Klous P, Braem C, Splinter E, Dekker J, Cathala G, de Laat W, Forne T. 2007. Quantitative analysis of chromosome conformation capture assays (3C-qPCR). *Nat Protoc* **2**: 1722-1733.

He A, Pu WT. 2010. Genome-wide location analysis by pull down of in vivo biotinylated transcription factors. *Curr Protoc Mol Biol* **Chapter 21**: Unit 21.20.

Kagey MH et al. 2010. Mediator and cohesin connect gene expression and chromatin architecture. *Nature* **467**: 430-435.

Kharchenko PV, Tolstorukov MY, Park PJ. 2008. Design and analysis of ChIP-seq experiments for DNA-binding proteins. *Nat Biotechnol* **26**: 1351-1359.

Kong Y. 2011. Btrim: a fast, lightweight adapter and quality trimming program for next-generation sequencing technologies. *Genomics* **98**: 152-153.

Kundaje A, Kyriazopoulou-Panagiotopoulou S, Libbrecht M, Smith CL, Raha D, Winters EE, Johnson SM, Snyder M, Batzoglou S, Sidow A. 2012. Ubiquitous heterogeneity and asymmetry of the chromatin environment at regulatory elements. *Genome Res* **22**: 1735-1747.

Langmead B, Trapnell C, Pop M, Salzberg SL. 2009. Ultrafast and memory-efficient alignment of short DNA sequences to the human genome. *Genome Biol* **10**: R25.

Lee TI, Johnstone SE, Young RA. 2006. Chromatin immunoprecipitation and microarray-based analysis of protein location. *Nat Protoc* **1**: 729-748.

McLean CY, Bristor D, Hiller M, Clarke SL, Schaar BT, Lowe CB, Wenger AM, Bejerano G. 2010. GREAT improves functional interpretation of cis-regulatory regions. *Nat Biotechnol* **28**: 495-501.

Newburger DE, Bulyk ML. 2009. UniPROBE: an online database of protein binding microarray data on protein-DNA interactions. *Nucleic Acids Res* **37**: D77-82.

Portales-Casamar E, Thongjuea S, Kwon AT, Arenillas D, Zhao X, Valen E, Yusuf D, Lenhard B, Wasserman WW, Sandelin A. 2010. JASPAR 2010: the greatly

expanded open-access database of transcription factor binding profiles. *Nucleic Acids Res* **38**: D105-10.

Reddy TE et al. 2012. Effects of sequence variation on differential allelic transcription factor occupancy and gene expression. *Genome Res* **22**: 860-869.

Saldanha AJ. 2004. Java Treeview--extensible visualization of microarray data. *Bioinformatics* **20**: 3246-3248.

Song L, Crawford GE. 2010. DNase-seq: a high-resolution technique for mapping active gene regulatory elements across the genome from mammalian cells. *Cold Spring Harb Protoc* **2010**: pdb.prot5384.

Trapnell C, Williams BA, Pertea G, Mortazavi A, Kwan G, van Baren MJ, Salzberg SL, Wold BJ, Pachter L. 2010. Transcript assembly and quantification by RNA-Seq reveals unannotated transcripts and isoform switching during cell differentiation. *Nat Biotechnol* **28**: 511-515.

Xu J, Sankaran VG, Ni M, Menne TF, Puram RV, Kim W, Orkin SH. 2010. Transcriptional silencing of {gamma}-globin by BCL11A involves long-range interactions and cooperation with SOX6. *Genes Dev* **24**: 783-798.

A

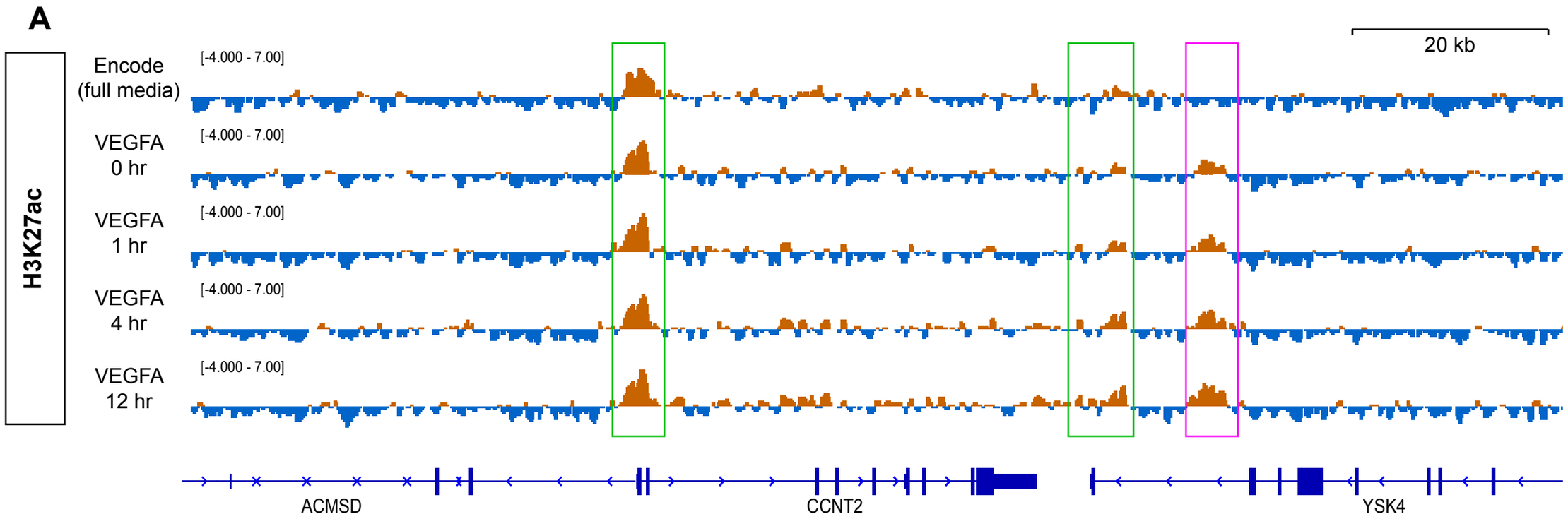

B

	Hour 0	Hour 1	Hour 4	Hour 12	ENCODE
Hour 0	1.000	0.905	0.864	0.841	0.497
Hour 1	0.905	1.000	0.882	0.858	0.480
Hour 4	0.864	0.882	1.000	0.910	0.501
Hour 12	0.841	0.858	0.910	1.000	0.466
ENCODE	0.497	0.480	0.501	0.466	1.000

Suppl. Fig. 1. H3K27ac ChIP-seq data in full media (ENCODE) compared to serum starvation followed by VEGFA stimulation. A. Representative browser view. Green boxes indicate H3K27ac patterns consistent between our data and ENCODE. Red boxes indicate divergent H3K27ac patterns. **B.** Pearson correlation coefficient between H3K27ac datasets in this study (Hours 0-12) and ENCODE data. Correlation coefficient was calculated by dividing the genome into 200 bp windows.

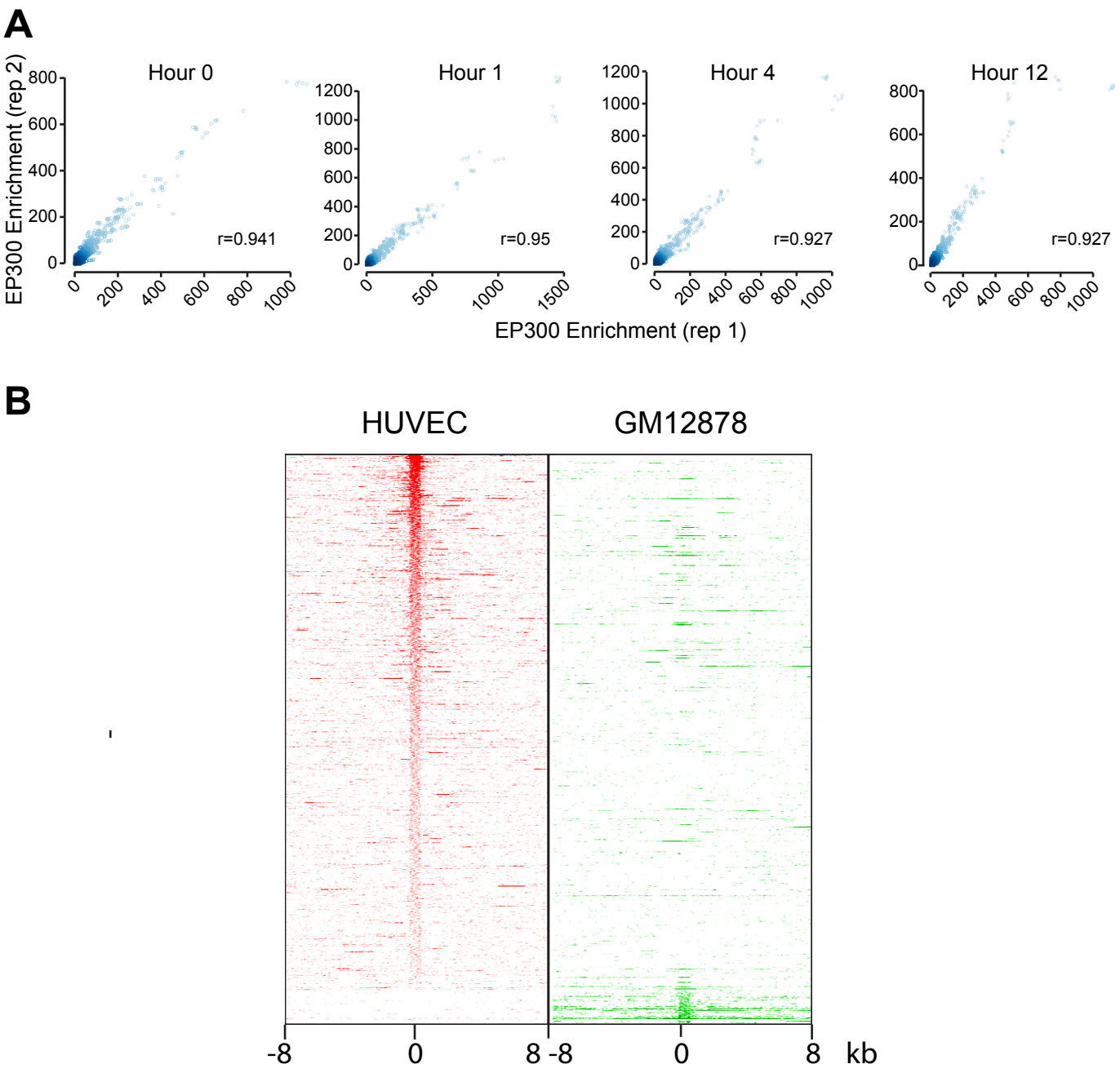

Suppl. Fig. 2. EP300 chromatin occupancy in HUVEC cells. A. Correlation between biological replicate EP300 ChIP-seq experiments. **B**. EP300 sites in HUVEC cells compared to GM12878. Rows represent 8 kb regions centered on p300 sites in GM12878 orHUVEC (union of peaks at all VEGFA time points). Few regions of EP300 enrichment were shared between GM12878 and HUVEC.

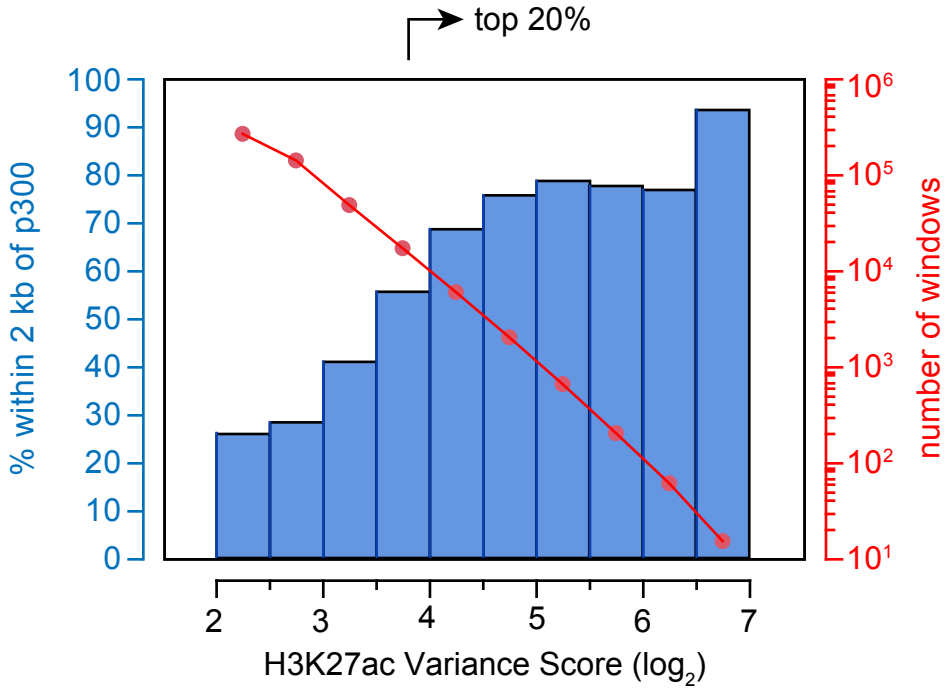

Suppl. Fig. 3. H3K27ac variance score and frequency of nearby p300 sites. The variance score of H3K27ac enrichment in 200 bp genomic windows was calculated. The plot shows the number of windows with a given variance score (red) and the frequency of they occur within 2 kb of p300 (blue). The peaks in the top 20th percentile of H3K27ac variance scores are indicated.

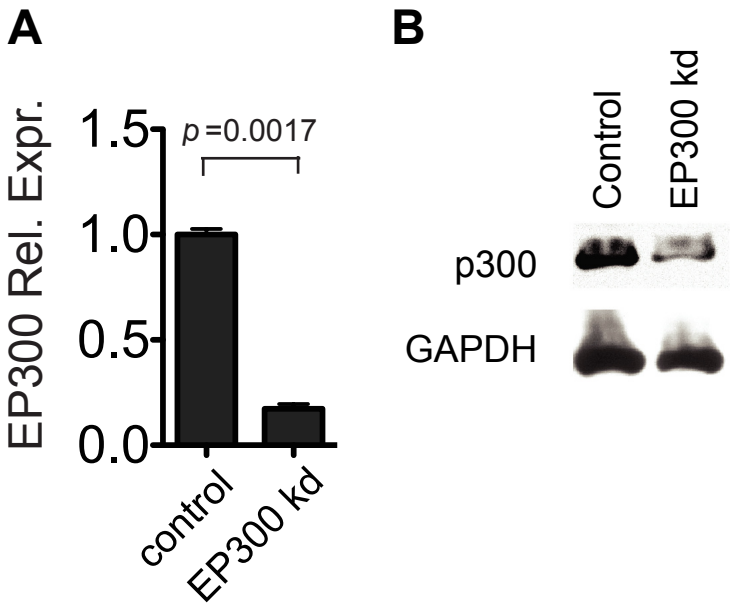

Suppl. Fig. 4. EP300 knockdown by siRNA.
HUVEC cells were transfected with siRNA directed against EP300 or control. EP300 RNA and protein were measured by qRTPCR (**A**) or western blotting (**B**).

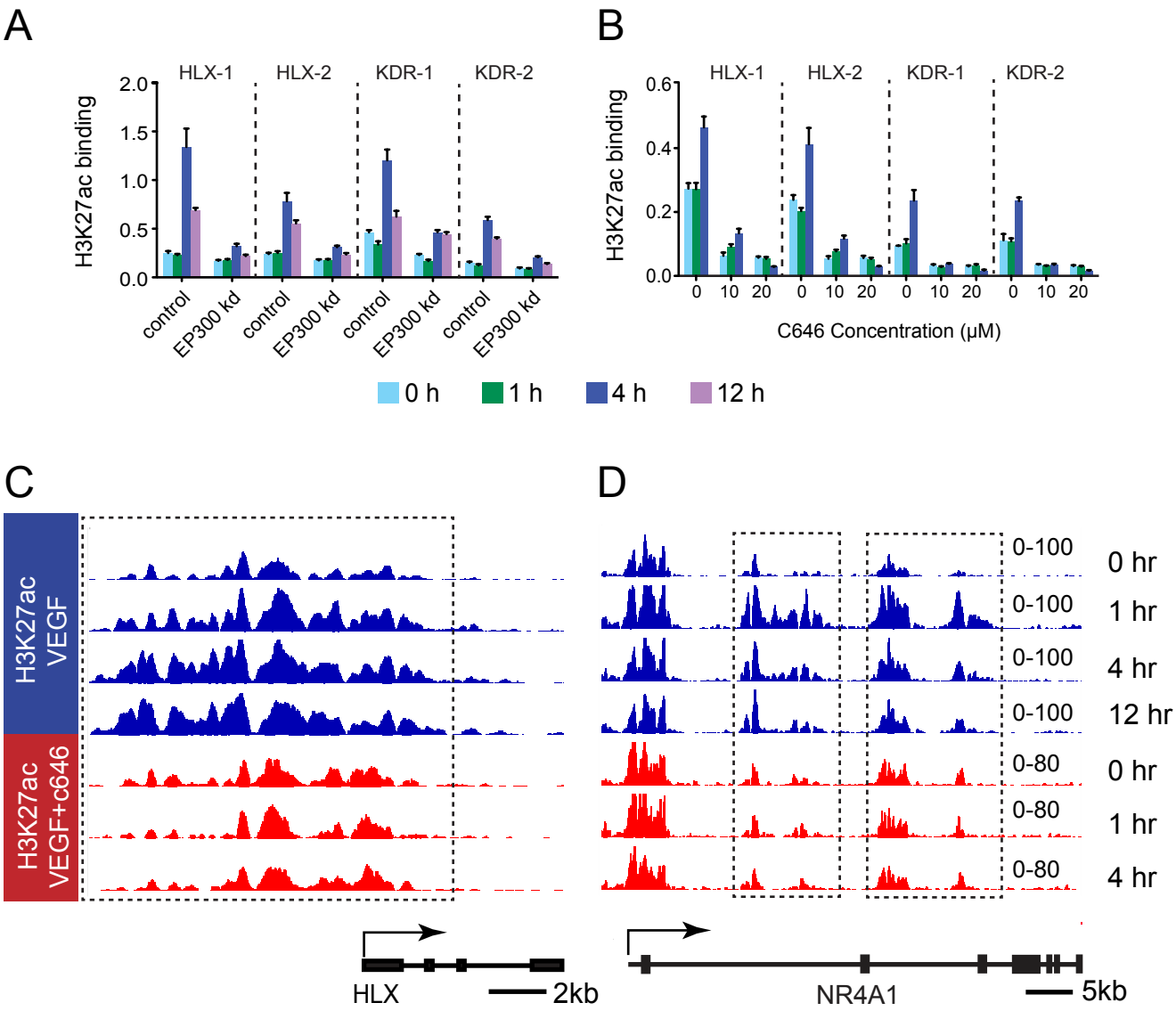

Suppl. Fig. 5. Inhibition of VEGFA-induced H3K27 acetylation changes by the EP300 inhibition. A. EP300 siRNA knockdown blunted H3K27ac changes induced by VEGF-A at 4 tested loci (HLX-1, HLX-2, KDR-1, and KDR-2). **B.** EP300 inhibition with the small molecule inhibitor C646 similarly blunted H3K27ac changes induced by VEGF-A at the 4 tested loci. **C-D.** Browser view corresponding to Fig. 1A-B. Dynamic H3K27ac regions are outlined by dotted lines. C646 blunded VEGF-A induced H3K27ac changes.

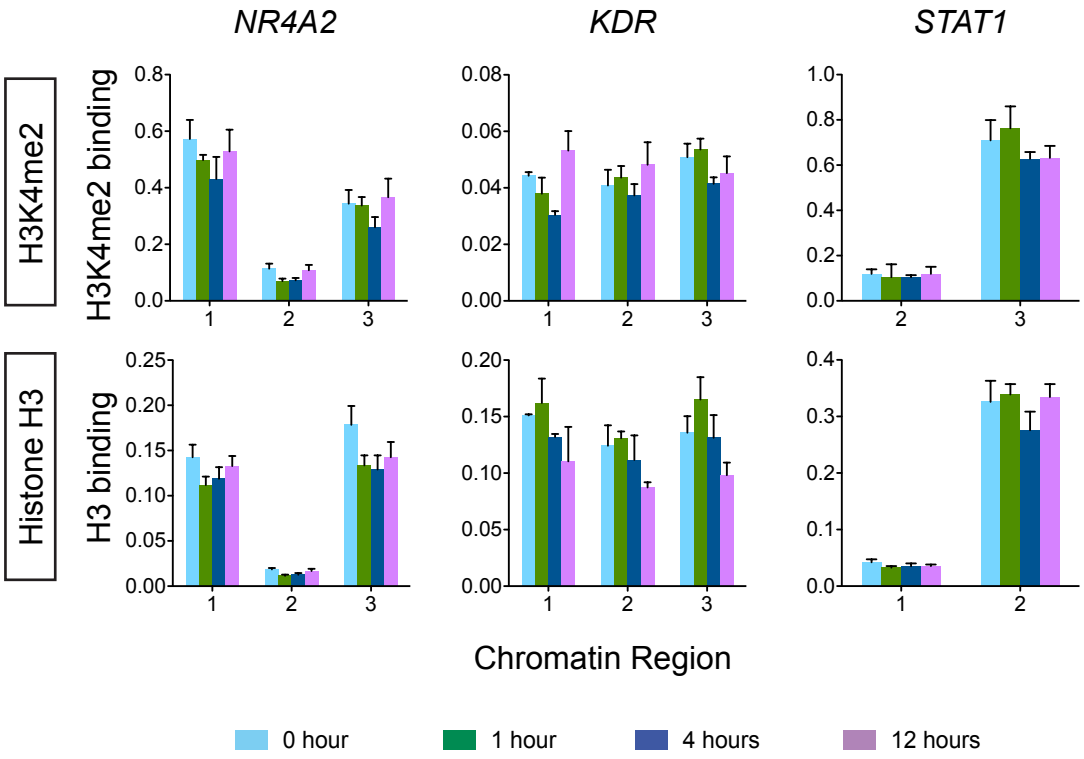

Suppl. Fig. 6. Chip-qPCR of H3K4me2 and histone H3 binding at dynamic H3K27ac sites. Numbered chromatin regions are indicated in Fig. 1D.

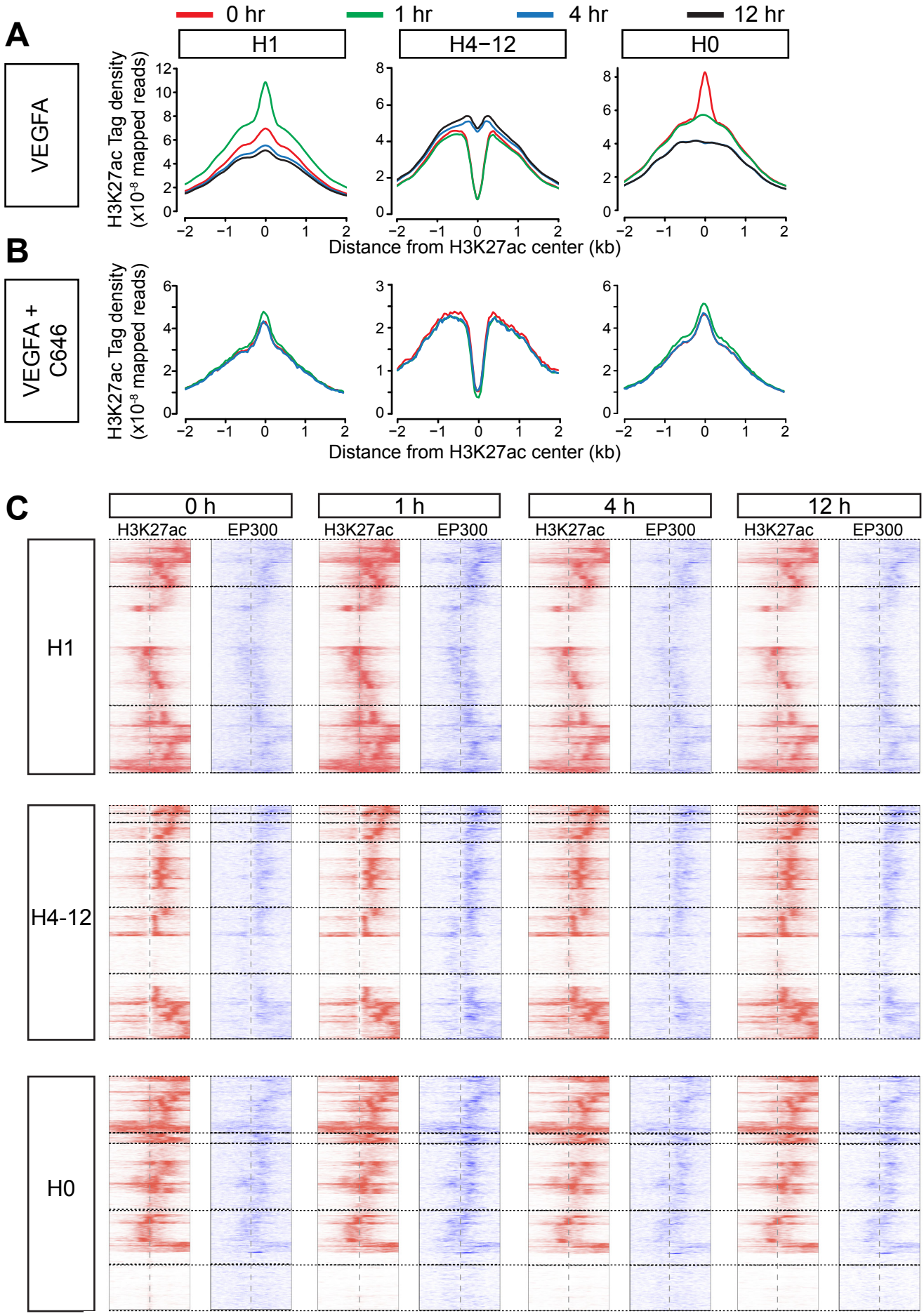
A
VEGFA
0 hr
1 hr
4 hr
12 hr
H1
H4−12
H0
H3K27ac Tag density (x10⁻⁸ mapped reads)
Distance from H3K27ac center (kb)
B
VEGFA + C646
H3K27ac Tag density (x10⁻⁸ mapped reads)
Distance from H3K27ac center (kb)
C
0 h
1 h
4 h
12 h
H3K27ac
EP300
H1
H4-12
H0

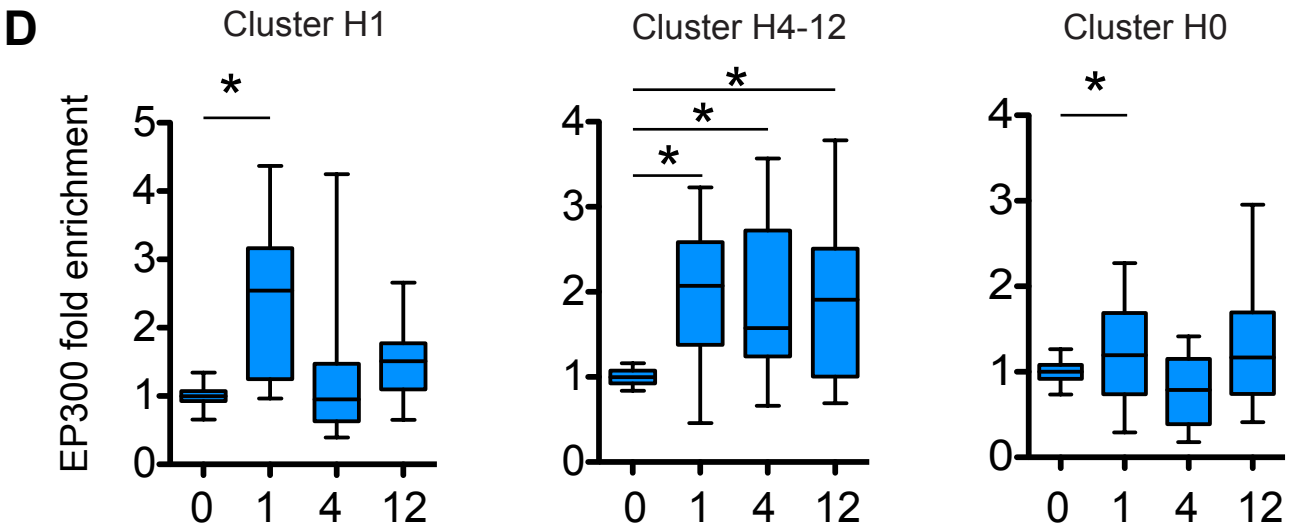

Suppl. Fig. 7. Dynamic, p300-associated, H3K27ac sites. These sites are in the top 20% of H3K27ac variance scores and are within 2 kb of p300. Time points indicate number of hours that HUVEC cells were treated with VEGFA, after 12 hours of serum starvation.
A. Aggregation plots of H3K27ac tag density in H1, H4-12, and H0 clusters.
B. Analogous aggregation plots as in A, but HUVECs were pretreated with EP300 inhibitor C646 prior to VEGFA stimulation. Note loss of VEGFA-induced changes in H3K27ac. C646 samples were collected at 0, 1, and 4 hour, but not 12 hour, timepoints.
C. Tag heat maps of H3K27ac enrichment in VEGFA-treated HUVECs, analyzed using an algorithm for functional strand clustering. Horizontal dotted lines indicate demark separate clusters. Vertical dotted lines indicate the center of the dynamic H3K27ac region. Note that H3K27ac enrichment was predominantly asymmetric around the center of the dynamic site.
D. Chip-qPCR validation of VEGFA-stimulated EP300 binding. Six different regions within each cluster were measured at each time point. Middle line indicates median, boxes indicate quartiles, and whiskers indicate min/max values. *, $p < 0.05$.

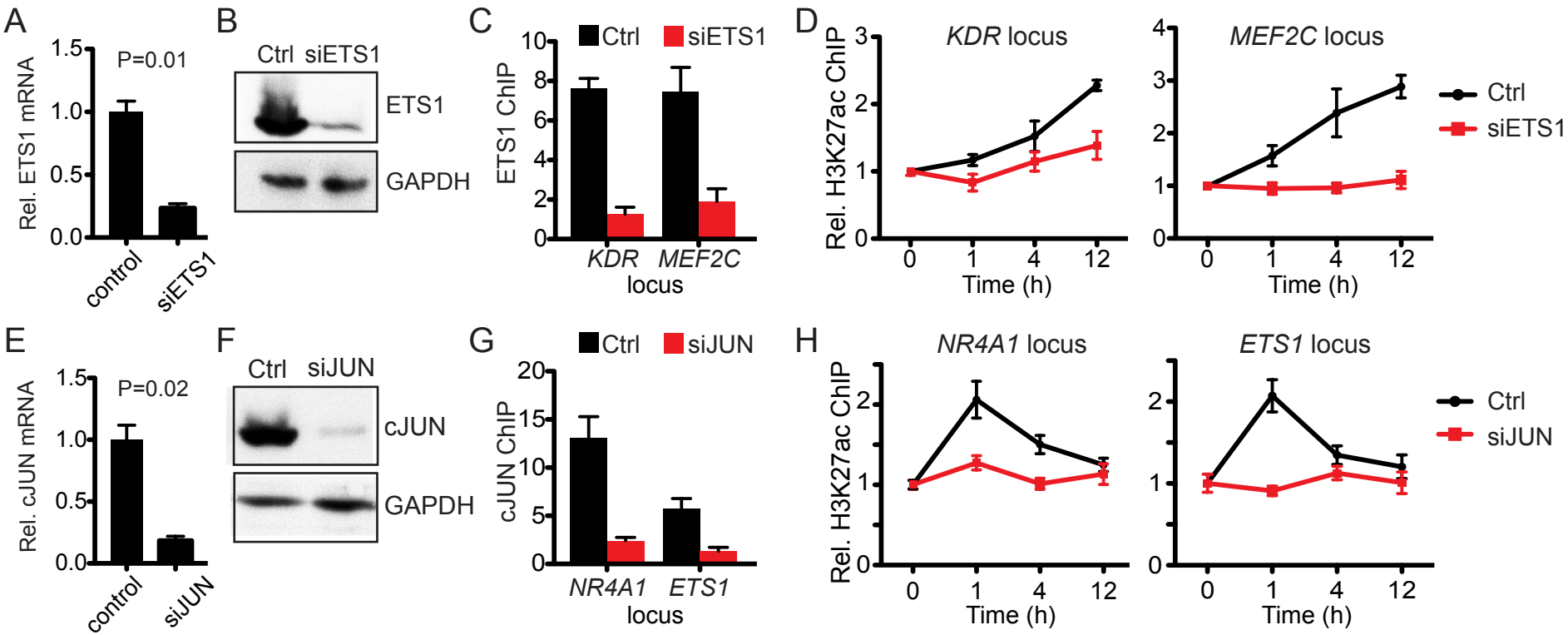

Suppl. Fig. 8. ETS1 and cJUN promoted H3K27ac changes at tested sites. A-B. mRNA and protein knockdown of ETS1 by transfection of HUVEC with specific or control siRNA. **C.** Enrichment of ETS1 at loci near *KDR* and *MEF2C* loci in control or siETS1 treated HUVEC. siETS1 reduced ETS1 occupancy ofthese sites. **D.** Relative H3K27ac enrichment at loci near *KDR* and *MEF2C* in control or siETS1 treated HUVEC. siETS1 blocked the increase of H3K27ac at these sites. **E-F.** mRNA and protein knockdown of cJUN by transfection of HUVEC with specific or control siRNA. **G.** Enrichment of cJUN at loci near *NR4A1* and *ETS1* loci in control or siJUN treated HUVEC. siJUN reduced cJUN occupancy of these sites. **H.** Relative H3K27ac enrichment at loci near *NR4A1* and *ETS1* in control or siJUN treated HUVEC. siETS1 blocked the increase of H3K27ac at these sites.

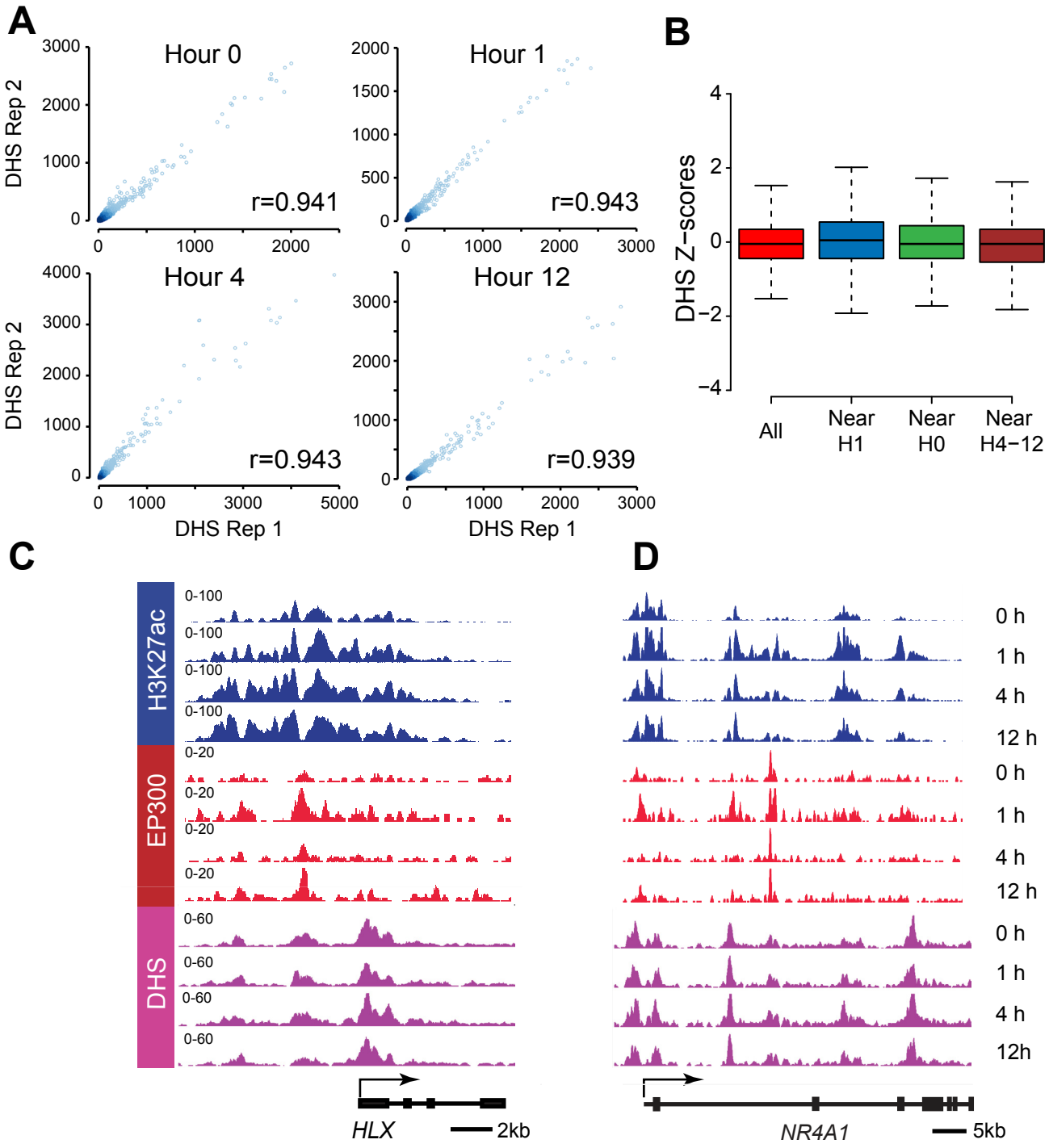

Suppl. Fig. 9. VEGFA stimulation did not significantly change chromatin accessibility near dynamic, EP300-associated H3K27ac sites. Chromatin accessibility was measured by sensitivity to DNase I digestion. **A.** Correlation between biological duplicates. **B**. Box plot of DNase-seq variation during the VEGFA stimulation time course, across the genome (All) or within 2 kb of members of H1, H4-12, or H4-12 H3K27ac clusters. DNase-seq reads at each time point during VEGFA stimulation were mapped to 200 bp windows. For each window with a mean of at least 10 reads, the z-score of the var/mean was calculated. Line, box, and whiskers represent the median, 25th and 75th quartiles, and 1.5 times the interquartile distance, respectively. Dynamic H3K27ac sites had no greater change over the time course than unselected DHS sites. **C-D**. Browser images of DHS signal at sites of significant H3K27ac variation. Note that DHS signal did not significantly change during the VEGFA stimulation time course.

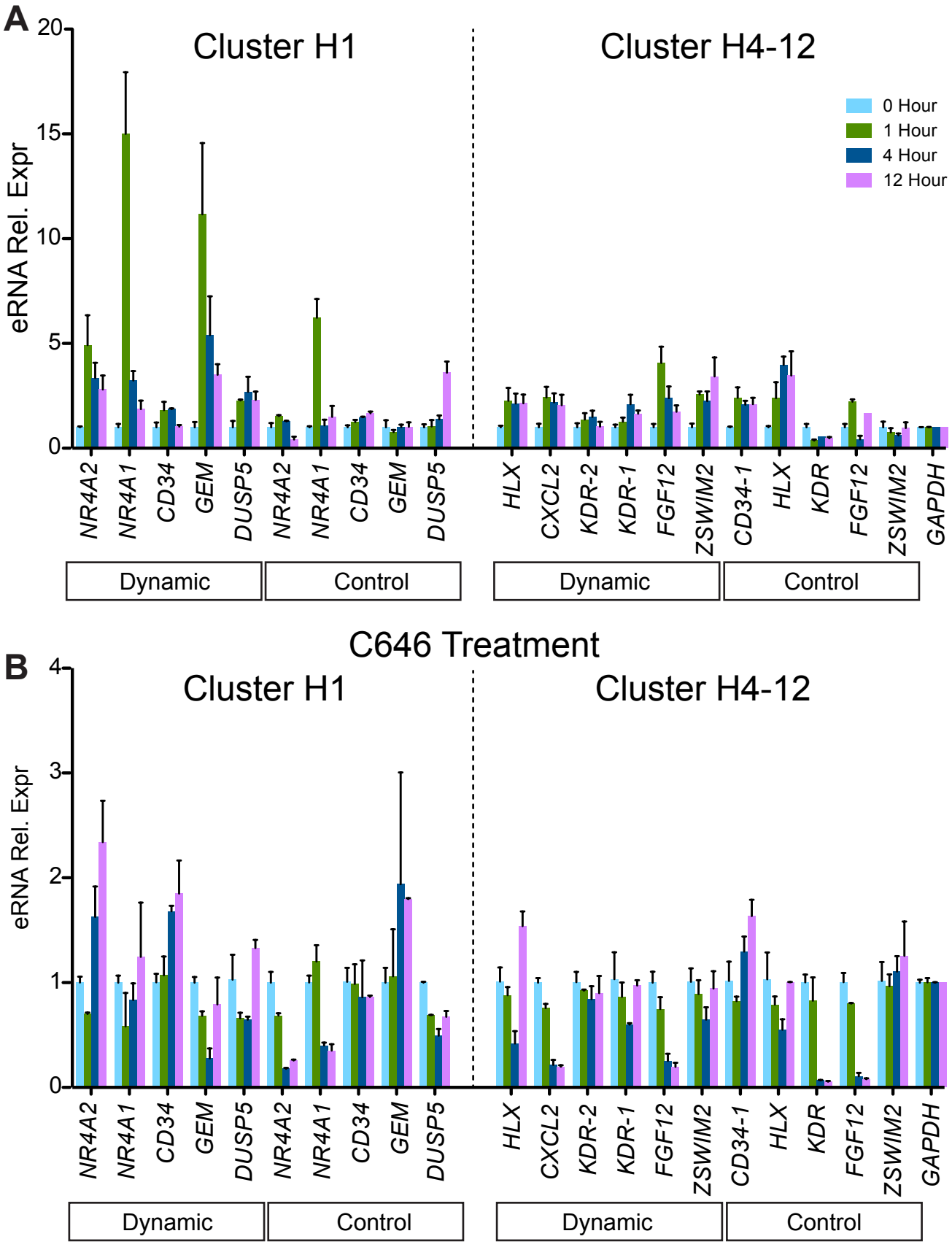

Suppl. Fig. 10. Dynamic H3K27ac sites expressed VEGFA-responsive eRNA. A. qRTPCR of eRNA expression at dynamic H3K27ac sites in the H1 or H4-12 clusters. Control indicates nearby regions with H3K27ac that did not score among the most highly variant H3K27ac sites. **B**. qRT-PCR of eRNA expression at the sites studied in (A), in the presence of the EP300 acetyltransferase inhibitor C646.

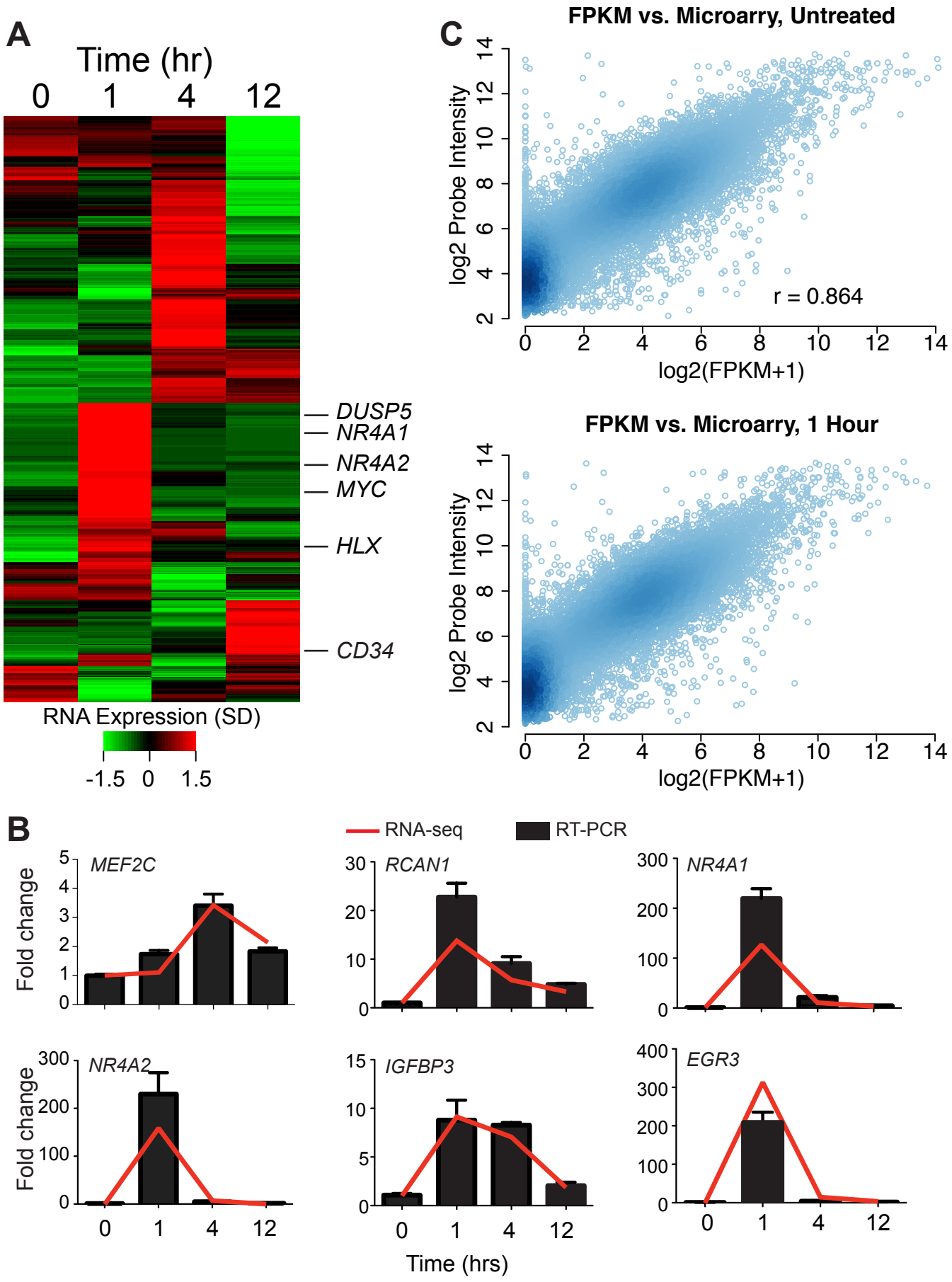

Suppl. Fig. 8. RNA expression after VEGFA stimulation. A. Hierarchically clustered heatmap of differentially expressed genes during VEGFA treatment of HUVEC cells. Several genes that were associated with dynamic H3K27ac loci that we studied are indicated. **B**. qRTPCR validation of differential gene expression following VEGFA treatment. **C**. Comparison of RNA-seq and published microarray RNA expression data (GSE15464 and GSE10778). Results were generally concordant between these methods. Pearson correlation coefficient is indicated.

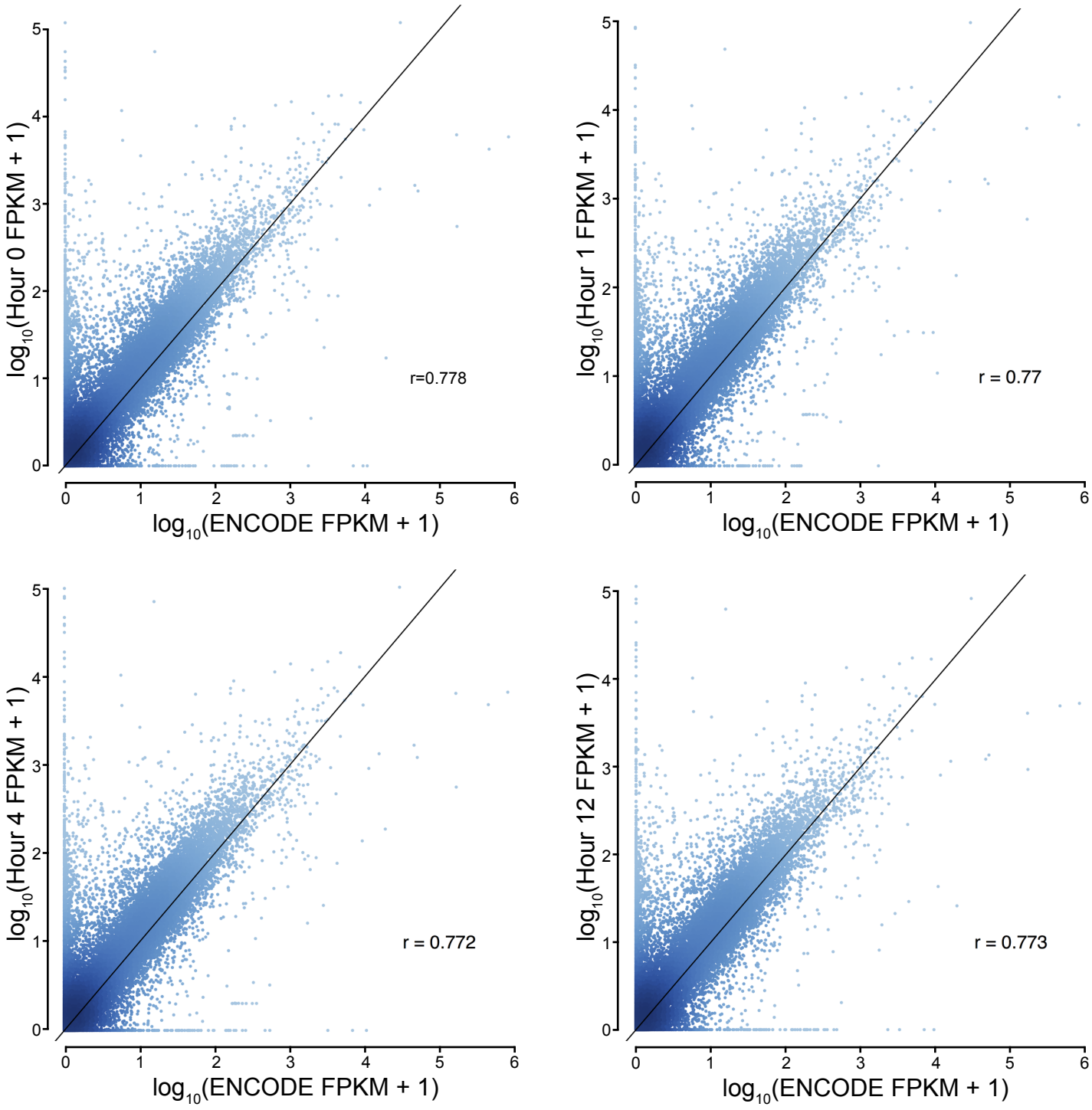

Suppl. Fig. 12. RNA-seq measurement of HUVEC gene expression during VEGFA stimulation, compared to ENCODE data in full endothelial growth media. Y-axis indicates data from this study, obtained after 12 hours of growth factor and serum withdrawl, followed by VEGFA treatment for 0, 1, 4, or 12 hours. X-axis indicates the ENCODE HUVEC data. r is the Spearman correlation coefficient for the unfiltered data.

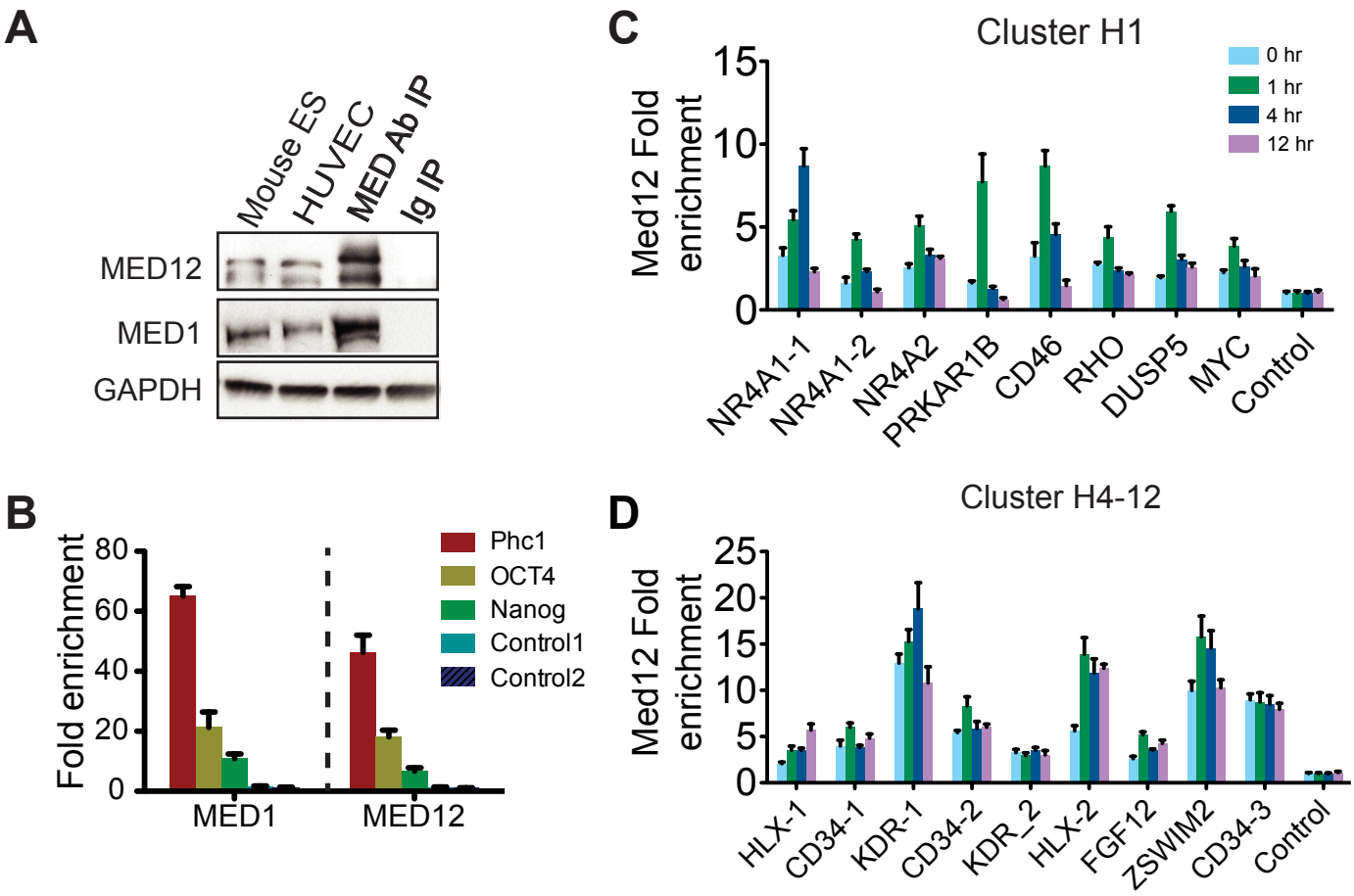

Suppl. Fig. 13. RNA expression and Mediator chromatin occupancy after VEGFA stimulation. A. Mediator 1 and 12 (MED1 and MED12) expression in HUVEC cells. ES cells were used as control. Immunoprecipitation was performed with the corresponding MED antibody. MED1 and MED12 expression in HUVEC was equivalent to ES cells. **B**. Chip-qPCR validating the specificity and affinity of MED1 and MED12 antibodies in ChIP using previously reported loci in mouse embryonic stem cells. **C-D**. MED12 Chip-qPCR of H3K27ac dynamic sites belonging to the H1 or H4-12 clusters. VEGFA stimulated MED12 occupancy of H3K27ac dynamic loci.